

# Direct evidence of void induced structural relaxations in colloidal glass formers

Cho-Tung Yip<sup>1</sup>, Masaharu Isobe<sup>2</sup>, Chor-Hoi Chan<sup>1</sup>, Simiao Ren<sup>1,3</sup>, Kin-Ping Wong<sup>3</sup>,  
Qingxiao Huo<sup>1</sup>, Chun-Sing Lee<sup>3</sup>, Yuen-Hong Tsang<sup>3</sup>, Yilong Han<sup>4</sup>, and Chi-Hang Lam<sup>3\*</sup>

<sup>1</sup>*Department of Physics, Shenzhen Graduate School,  
Harbin Institute of Technology, Shenzhen 518055, China*

<sup>2</sup>*Graduate School of Engineering, Nagoya Institute of Technology, Nagoya, 466-8555, Japan*

<sup>3</sup>*Department of Applied Physics, Hong Kong Polytechnic University, Hung Hom, Hong Kong, China*

<sup>4</sup>*Department of Physics, Hong Kong University of Science and Technology, Clear Water Bay, Hong Kong, China*

(Dated: November 5, 2020)

Particle dynamics in supercooled liquids are often dominated by string-like motions in which lines of particles perform activated hops cooperatively. The structural features triggering these motions, crucial in understanding glassy dynamics, remain highly controversial. We experimentally study microscopic particle dynamics in colloidal glass formers at high packing fractions. With a small polydispersity leading to glass-crystal coexistence, a void in the form of a vacancy in the crystal can diffuse reversibly into the glass and further induces string-like motions. In the glass, a void takes the form of a quasi-void consisting of a few neighboring free volumes and is transported by the string-like motions it induces. In fully glassy systems with a large polydispersity, similar quasi-void actions are observed. The mobile particles cluster into string-like or compact geometries, but the compact ones can further be broken down into connected sequences of strings, establishing their general importance.

The microscopic origin of kinetic arrest and relaxation mechanisms in deeply supercooled glassforming liquids have been debated actively for decades [1, 2]. Optical microscopy experiments on colloidal liquids play an important role because detailed motions of individual particles are accessible [3]. An important progress has been the experimental confirmation of string-like motions [4–7], first discovered in molecular dynamics (MD) simulations [8]. During a string-like event, particles arranged in a line hop to replace the preceding ones. It can be portrayed by a string of participating particles [7–9] or by a smooth line formed by the joint trajectories of these particles [4, 10, 11]. A synchronous segment of a string is called a micro-string [9], which has been suggested as elementary relaxations in glasses [11–13]. Theoretically, free volumes [14] are widely believed to play a pivotal role in glassy dynamics. In particular, voids, i.e. free volumes each of roughly the size of a particle, have long been studied [15] and are often applied to explain glassy phenomena [16]. However, voids of sizes comparable to the particles show only small correlations to particle dynamics [10, 17, 18].

We study colloidal liquid sandwiched between two glass plates. Glass-crystal coexisting and glassy systems are obtained using particle size distributions following unimodal (average diameter  $3.77\mu\text{m}$ ) and bimodal (average diameters  $3.77\mu\text{m}$  and  $4.62\mu\text{m}$ ) forms respectively. They are small enough to exhibit strong Brownian motions, but are larger than those in typical experiments [4–7] in order to guarantee a perfect monolayer arrangement of particles upon sinking to the lower plate, forming a quasi-two-dimensional system. For all results reported here, all particles are practically identified by image analysis soft-

ware. Their slower movements due to the relatively large particle sizes also enable snapshots taken at rates much faster than the dynamics so that time-averaged particle positions are very accurately measured. We study particle dynamics close to the relaxation time even at a packing fraction, in our knowledge, higher than those used in similar hard sphere experiments previously [4–7]. This requires imaging in a single experiment for up to  $10^6\text{s}$ , compared with typical durations of an hour or less. See the supplementary information for details [30].

Figure 1(a) shows time-colored coarse-grained particle trajectories [11] covering a period  $T_{\text{traj}}$  in a glassy colloidal system with bimodal particle sizes at the highest packing fraction  $\phi = 0.80$ . The trajectory of particle  $i$  is based on its coarse-grained position  $\mathbf{r}_i^c(t)$  at time  $t$  obtained by averaging its instantaneous position  $\mathbf{r}_i$  over a coarsening time  $\Delta t_c$ , i.e.  $\mathbf{r}_i^c(t) = \langle \mathbf{r}_i(t') \rangle_{t' \in [t, t + \Delta t_c]}$ . It is plotted by joining consecutive positions  $\mathbf{r}_i^c(t)$  and  $\mathbf{r}_i^c(t + \Delta t_c)$  within time  $T_{\text{traj}}$  with line segments colored according to  $t$ . From Fig. 1(a), a feature characteristic at high  $\phi$  is a strong mobility contrast with highly mobile particles neighboring nearly stationary ones. This is verified by MD simulations of hard disks. (See SI for more detailed experimental and simulations results [30].) We also observe string-like motions [8] revealed as smoothly connected trajectories of the mobile particles [4, 10, 11]. All results presented in the followings are based on coarse-grained particle positions and trajectories. Figure 1(b)-(c) magnifies the coarse-grained trajectories showing a typical string-like motion. The initial and final particle configurations of the period are also shown. The time-coloring approach conveniently illustrate if the motions are synchronous [11]. For example, the string in Fig. 1(b)-(c) is asynchronous and consists of three micro-strings [9] colored in red, yellow and green.

The high mobility contrast among particles allows easy

\* Email: [C.H.Lam@polyu.edu.hk](mailto:C.H.Lam@polyu.edu.hk)

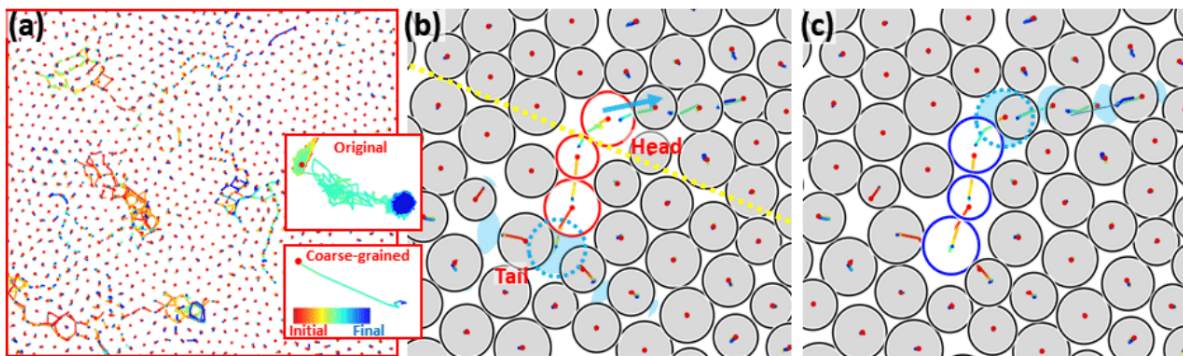


FIG. 1. (a) Coarse-grained particle trajectories at packing fraction  $\phi = 0.80$  over a duration  $T_{traj} = 10^6$  s. Line segments in trajectories are colored according to the times of occurrence. Initial positions are denoted by red dots. Trajectories of hopped particles connect smoothly, revealing string-like motions. Inset: Magnified views of the original and the coarse-grained trajectories of a typical particle. (b) and (c) Coarse-grained trajectories for duration  $T_{traj} = 20000$  s showing a typical string-like particle hopping motion. Particle configurations at the beginning (b) and the end (c) of the period are also shown. A quasi-void consisting of fragmented free volumes (blue areas) is transported by the string across a line of otherwise stationary particles (yellow dotted line). Note that the blue dotted circles show the final position of the particle at the string tail in (b) and the initial position of the particle at the string head in (c).

interpretation of the flow of mass and hence also of free-volume. Noting that a hopping particle nearly completely replaces the preceding one and adjacent non-hopping particles are practically stationary, a free volume comparable to the typical particle size is transported by the string through any cross-section of the sample penetrated by the string, e.g. yellow dotted line in Fig. 1(b). For convenience, we designate the direction of a string along the free volume flow direction and that a string points from its tail to head, so that subsequent extension of the string emerges from the head. Importantly, a continuous free volume of a particle size is not observed, consistent with previous studies [10, 17, 18]. Instead, the transported free volume is fragmented and distributed among a few neighboring interstitial areas both before and after the motion as schematically illustrated in Fig. 1(b)-(c). Despite fragmented, the coupled free volumes are transported in whole and behave as a quasi-particle, which we refer to as a quasi-void [11]. Further explanation of quasi-void is discussed in SI [30].

The physical relevance of a quasi-void is directly evident from its reversible conversion into a vacancy, an established quasi-particle. Figure 2(a) shows particle trajectories in a unimodal colloidal system with coexisting glassy and crystalline regions. A single string-like motion traverses between the phases. Figure 2(b)-(f) shows the detailed sequence of events. In the crystal, the trajectories of adjacent hopping particles smoothly connect to form a continuous line, which can be self-crossing and backtracking occasionally. We refer to these joint trajectories in the crystal also as strings, generalizing the usual definition of string-like motions. The vacancy induces such string-like motions during which it is transported from tail to head, analogous to the description above for quasi-voids. Importantly, the string extends remarkably smoothly across the glass-crystal interface.

Remarkably, the excellent continuity of the string even across the phase boundary in Fig. 2(a) directly shows that the string-like motion in the glassy region is ultimately caused by the vacancy. The vacancy upon entering the glass turns into a quasi-void, which is thus essentially a dressed vacancy. We refer to both as a void, which manifests itself as a quasi-void or vacancy in a glass or crystal respectively.

String-like motions have been suggested to diminish in importance against compact rearranging groups as supercooling deepens [7, 19]. To study it critically, we classify the mobile particles as string-like and core-like and reproduce the trend of an increasing density of core-like particles as observed previously [7] (see SI [30]). Figure 3(a) shows the coarse-grained trajectories in a region with a typical core-like group. In sharp contrast to suggestions in [7], they can however be broken down into two sequences of string-like motions induced by two quasi-voids as shown in Fig. 3(b)-(k). More examples are shown in the SI. This fully supports that strings dominate relaxations even at deep supercooling [11–13]. The apparent core-like geometries in fact result from an increased dynamic heterogeneity so that strings are more localized and overlap each other. This is also observed in our lattice model of glass characterized by void dynamics [20].

We now study particle hopping statistics. A particle is considered hopped if its coarse-grained displacement exceeds  $0.8\sigma$  ( $\sigma = 3.77\mu\text{m}$ ), which equals the position of the dip in the van Hove self-correlation function (see SI [30]). At a large packing fraction  $\phi$ , dynamics is dominated by particle activated hops organized as strings. Collective flows typical of non-glassy liquids however still exist locally in a diminished role. To quantify this, we measure a correlation  $Y$  of the displacements  $\Delta r_i$  and  $\Delta r_j$  of a hopping particle and its neighbors during a time  $\delta t$ , defined



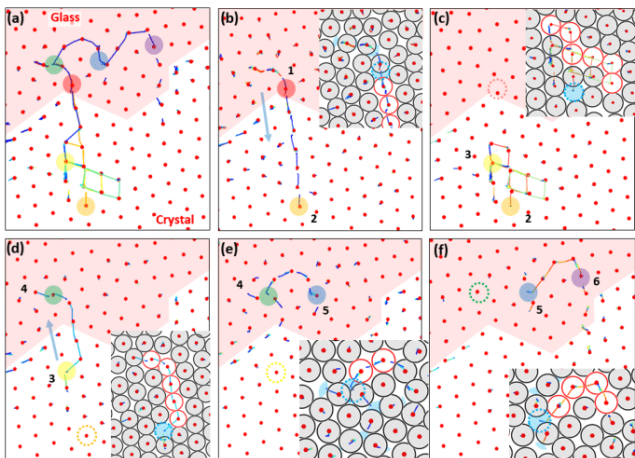


FIG. 2. Coarse-grained particle trajectories covering a time  $T_{traj} = 29120s$  from a unimodal colloidal system with a small size dispersion exhibiting coexisting glassy (white) and crystalline (red) regions with  $\phi = 0.81$  and  $0.83$  respectively. (a) A single string-like motion traverses remarkably smoothly across both regions, depicting the motion of a void. (b-f) The same trajectories as in (a) split up over consecutive time sub-intervals showing detailed motions. Numbered circles mark the initial and final positions of the void at the time sub-intervals. (b) A void moves from the glass to the crystal (blue arrow) and (c) diffuses along lattice edges. (d) It moves back to the glass (blue arrow) and (e-f) induces a sequence of two micro-string motions. Insets in (b-f): Trajectories shown together with initial particle configurations of the time sub-interval. The void takes the form of a vacancy (blue solid circles) in the crystal (c-d) and a quasi-void with fragmented free volumes (blue areas) in the glass (b,e,f).

by

$$Y = \left\langle \min \{ \Delta r_j \}_{j \in \Omega_i} / \Delta r_i \right\rangle_{i \in \Omega_{hop}}, \quad (1)$$

where the minimization is performed over the set  $\Omega_i$  of nearest neighbors of particle  $i$  while the average is over the set  $\Omega_{hop}$  of all hopped particles. Figure 4(a) plots  $Y$  against  $\phi$ . As  $\phi$  increases,  $Y$  decreases towards 0, corresponding to the limiting case of particle hops in a background of stationary particles and thus an absence of collective flow. The decline of  $Y$  to a small value is verified by our MD simulations (see SI [30]). Our result again supports the dominant nature of string-like hopping motions under deep supercooling. It also shows the importance of adopting a large  $\phi$  for suppressing collective flow in order to access true glassy dynamics.

Theoretical descriptions of void induced dynamics traditionally assume free diffusion of voids [15]. However, we observe strong temporal correlations as revealed by abundant back-and-forth particle hopping motions. They occur not only in our glassy systems but also in the crystalline regions, noting that our unimodal system also admits a small particle size dispersion and hence a non-trivial free energy landscape. Such memory effects is exemplified in the reversed motions in Fig. 2(d) versus those

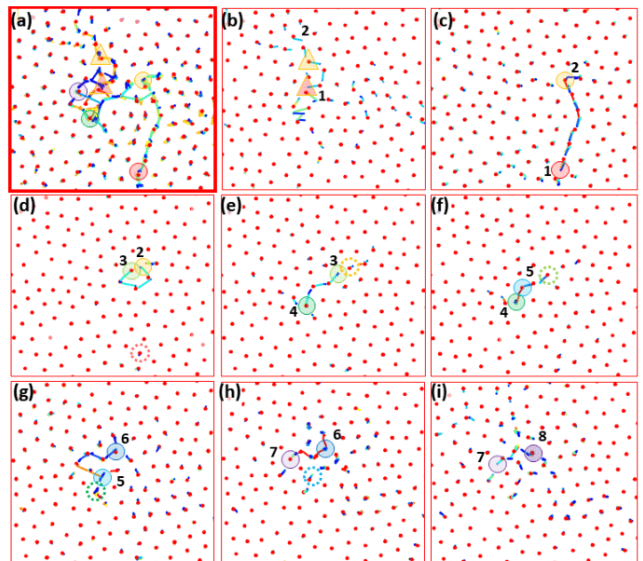


FIG. 3. (a) Coarse-grained trajectories in a region from Fig. 1(a) with a core-like cluster of mobile particles, as revealed by their highly interconnected trajectories. (b)-(i) Trajectories from (a) split up over consecutive time sub-intervals, showing two independent string-like motions in (b) and (c)-(i). Numbered triangles and circles mark initial and final positions of the two quasi-voids in each time sub-interval.

in Fig. 2(b). To quantify the temporal correlations, after a particle has hopped, we monitor its subsequent motions for a long time in order to calculate the probabilities  $P_{ret}$  and  $P_{esc} \simeq 1 - P_{ret}$  that it may next perform a returning hop to the original position or an escaping hop to a third position respectively. Results shown in Fig. 4(b) are in agreement with our MD simulations (see SI [30]) and provide an experimental confirmation to polymer and lattice simulation results [11, 20]. In particular,  $P_{ret}$  increases with  $\phi$  and reaches a high value of 0.8 at  $\phi = 0.80$ . Particle and void dynamics thus differ drastically from free

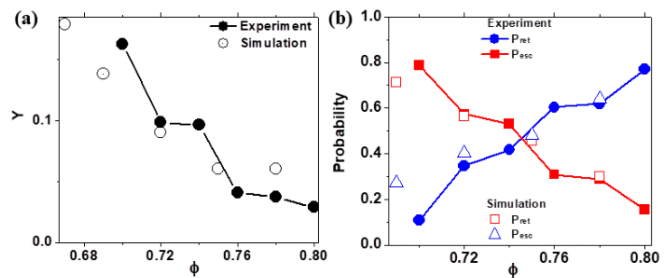


FIG. 4. (a) Displacement correlation  $Y$  measuring the mobility of the neighbors of a hopping particle. At large  $\phi$ , values tend towards 0, corresponding to existence of stationary neighbors for all hopping particles. (b) Returning and escaping probabilities,  $P_{ret}$  and  $P_{esc}$ , of hopped particles against  $\phi$ . They tend towards 1 and 0 respectively at large  $\phi$  corresponding to the dominance of back-and-forth hopping motions.

diffusion. A large  $P_{ret}$  supports that string-like hopping motions are mostly  $\beta$  relaxations and only a vanishingly small fraction of them, i.e. the escaping hops, are structural relaxations [11, 21]. A theory of glass accounting for these correlations has been suggested recently [22, 23].

Strings can extend step by step to long lengths as shown in Figs. (2) and (3). The extensions are always observed to emerge from the string heads rather than the tails, as is easily explained by the transport of the quasi-void from tail to head from which further propagations can occur. Moreover, the long string lengths imply good integrity and long lifetimes of the quasi-voids. This is unexpected because the fragmented free volumes constituting a quasi-void are not energetically bounded and apparently can be easily dispersed. We believe that once a quasi-void, which is usually isolated at a high  $\phi$ , is momentarily dispersed, the free-volume fragments become immobile. The likely evolution is then the reassembly of the quasi-void, a possibility guaranteed by the time-reversal symmetry of the underlining particle dynamics under local quasi-equilibrium conditions. The robustness of the quasi-voids distinguishes our description from a generic free-volume picture. Creation and annihilation of quasi-voids appear to occur mostly in highly active regions with multiple quasi-voids.

The void induced particle dynamics reported here is fundamentally a straightforward generalization of vacancy induced motions in crystals. Vacancies are also believed to be responsible for particle dynamics in high-entropy alloys in crystalline form, which show glass-like

sluggish dynamics [24]. Our work also explains the irrelevance of compact voids [17, 18], as they have lower entropies and should be statistically unfavorable compared with quasi-voids. Dynamics in glasses have been found to be correlated to soft spots and local structures [25–29]. These are consistent with our picture because the presence of a quasi-void clearly impacts the local softness and structures. The quasi-void notion may shed light on the evolution dynamics of these local properties, which is still lacking.

In conclusion, we have studied quasi-voids in glass formers consisting of fragmented free volumes, which induce and are transported by string-like particle hopping motions. Their relevance is evidenced by the reversible conversion of a quasi-void into a vacancy in a crystalline region. The induced string-like motions are shown to dominate relaxations even in deep supercooling. We have also presented quantitatively a reduced role of collective flow and drastically enhanced temporal correlations in particle motions as supercooling deepens.

We thank helpful discussions with D.A. Weitz and J.P. Garrahan. This work was supported by Shenzhen Municipal Science and Technology projects (Grant No. JCYJ 201803063000421), JSPS KAKENHI (Grant No. 17K05574, No. 20K03785), Hong Kong GRF (Grant No. 15330516), and National Natural Science Foundation of China (Grant No. 11974297). Part of the computations was performed at the Supercomputer Center, ISSP, Univ. of Tokyo.

- 
- [1] G. Biroli and J. P. Garrahan, “Perspective: The glass transition,” *J. Chem. Phys.* **138**, 12A301 (2013).
  - [2] F. H. Stillinger and P. G. Debenedetti, “Glass transition thermodynamics and kinetics,” *Annu. Rev. Condens. Matter Phys.* **4**, 263 (2013).
  - [3] E. R. Weeks, “Introduction to the colloidal glass transition,” *ACS Macro Letters* **6** (2017).
  - [4] A. H. Marcus, J. Schofield, and S. A. Rice, “Experimental observations of non-gaussian behavior and string-like cooperative dynamics in concentrated quasi-two-dimensional colloidal liquids,” *Phys. Rev. E* **60**, 5725 (1999).
  - [5] E. R. Weeks, J. C. Crocker, A. C. Levitt, A. Schofield, and D. A. Weitz, “Three-dimensional direct imaging of structural relaxation near the colloidal glass transition,” *Science* **287**, 627 (2000).
  - [6] Z. Zhang, P. J. Yunker, P. Habdas, and A. G. Yodh, “Cooperative rearrangement regions and dynamical heterogeneities in colloidal glasses with attractive versus repulsive interactions,” *Phys. Rev. Lett.* **107**, 208303 (2011).
  - [7] K. Hima Nagamanasa, S. Gokhale, A. K. Sood, and R. Ganapathy, “Direct measurements of growing amorphous order and non-monotonic dynamic correlations in a colloidal glass-former,” *Nat. Phys.* **11**, 403 (2015).
  - [8] C. Donati, J. F. Douglas, W. Kob, S. J. Plimpton, P. H. Poole, and S. C. Glotzer, “Stringlike cooperative motion in a supercooled liquid,” *Phys. Rev. Lett.* **80**, 2338 (1998).
  - [9] M. Aichele, Y. Gebremichael, F. W. Starr, J. Baschnagel, and S. C. Glotzer, “Polymer-specific effects of bulk relaxation and stringlike correlated motion in the dynamics of a supercooled polymer melt,” *J. Chem Phys.* **119**, 5290 (2003).
  - [10] S. Swayamjyoti, J. F. Löffler, and P. M. Derlet, “Local structural excitations in model glasses,” *Phys. Rev. B* **89**, 224201 (2014).
  - [11] C.-H. Lam, “Repetition and pair-interaction of string-like hopping motions in glassy polymers,” *J. Chem. Phys.* **146**, 244906 (2017).
  - [12] A. S. Keys, L. O. Hedges, J. P. Garrahan, S. C. Glotzer, and D. Chandler, “Excitations are localized and relaxation is hierarchical in glass-forming liquids,” *Phys. Rev. X* **1**, 021013 (2011).
  - [13] M. Isobe, A. S. Keys, D. Chandler, and J. P. Garrahan, “Applicability of dynamic facilitation theory to binary hard disk systems,” *Phys. Rev. Lett.* **117**, 145701 (2016).
  - [14] D. Turnbull and M. H. Cohen, “Free-volume model of the amorphous phase: glass transition,” *J. Chem. Phys.* **34**, 120 (1961).
  - [15] S. H. Glarum, “Dielectric relaxation of isoamyl bromide,” *J. Chem. Phys.* **33**, 639 (1960).
  - [16] Matteo Lulli, Chun-Shing Lee, Hai-Yao Deng, Cho-Tung

- Yip, and Chi-Hang Lam, “Spatial heterogeneities in structural temperature cause kovacs’ expansion gap paradox in aging of glasses,” *Physical Review Letters* **124**, 095501 (2020).
- [17] J. C. Conrad, F. W. Starr, and D. A. Weitz, “Weak correlations between local density and dynamics near the glass transition,” *J. Phys. Chem. B* **109**, 21235 (2005).
- [18] A. Widmer-Cooper and P. Harrowell, “Free volume cannot explain the spatial heterogeneity of debye–waller factors in a glass-forming binary alloy,” *J. Non-Cryst. Solids* **352**, 5098 (2006).
- [19] J. D. Stevenson, Jörg Schmalian, and P. G. Wolynes, “The shapes of cooperatively rearranging regions in glass-forming liquids,” *Nat. Phys.* **2**, 268 (2006).
- [20] L.-H. Zhang and C.-H. Lam, “Emergent facilitation behavior in a distinguishable-particle lattice model of glass,” *Phys. Rev. B* **95**, 184202 (2017).
- [21] H.-B. Yu, R. Richert, and K. Samwer, “Structural rearrangements governing johari-goldstein relaxations in metallic glasses,” *Sci. Adv.* **3**, e1701577 (2017).
- [22] C.-H. Lam, “Local random configuration-tree theory for string repetition and facilitated dynamics of glass,” *J. Stat. Mech.* **2018**, 023301 (2018).
- [23] H.-Y. Deng, C.-S. Lee, M. Lulli, L.-H. Zhang, and C.-H. Lam, “Configuration-tree theoretical calculation of the mean-squared displacement of particles in glass formers,” *J. Stat. Mech.* **2019**, 094014 (2019).
- [24] J.-W. Yeh, “Alloy design strategies and future trends in high-entropy alloys,” *JOM* **65**, 1759 (2013).
- [25] A. Widmer-Cooper, H. Perry, P. Harrowell, and D. R. Reichman, “Irreversible reorganization in a supercooled liquid originates from localized soft modes,” *Nat. Phys.* **4**, 711 (2008).
- [26] C. Patrick Royall and S. R. Williams, “The role of local structure in dynamical arrest,” *Phys. Rep.* **560**, 1 (2015).
- [27] E. D. Cubuk, S. S. Schoenholz, J. M. Rieser, B. D. Malone, J. Rottler, D. J. Durian, E. Kaxiras, and A. J. Liu, “Identifying structural flow defects in disordered solids using machine-learning methods,” *Phys. Rev. Lett.* **114**, 108001 (2015).
- [28] S. S. Schoenholz, E. D. Cubuk, D. M. Sussman, E. Kaxiras, and A. J. Liu, “A structural approach to relaxation in glassy liquids,” *Nat. Phys.* **12**, 469 (2016).
- [29] V. Bapst, T. Keck, A. Grabska-Barwińska, C. Donner, E. D. Cubuk, S. S. Schoenholz, A. Obika, A.W.R. Nelson, T. Back, D. Hassabis, and P. Kohli, “Unveiling the predictive power of static structure in glassy systems,” *Nat. Phys.* **16**, 448 (2020).
- [30] See Supplemental Material for the Materials and Methods and Other Supplementary Results, which includes Refs. [31–34].
- [31] J. C. Crocker and E. R. Weeks, Particle tracking using IDL, <http://www.physics.emory.edu/faculty/weeks/idl/tracking.html>
- [32] E. P. Bernard, W. Krauth, and D. B. Wilson, “Event-chain Monte Carlo algorithms for hard-sphere systems,” *Phys. Rev. E* **80**, 056704 (2009).
- [33] M. Isobe, “Simple and efficient algorithm for large scale molecular dynamics simulation in hard disk system,” *Int. J. Mod. Phys. C* **10**, 1281 (1999).
- [34] W. G Hoover, N. E. Hoover, and K. Hanson, “Exact hard-disk free volumes,” *J. Chem. Phys.* **70**, 1837 (1979).

# Supplementary Material for

**Title: Direct evidence of void induced structural relaxations in colloidal glass formers**

Authors: Cho-Tung Yip<sup>1</sup>, Masaharu Isobe<sup>2</sup>, Chor-Hoi Chan<sup>1</sup>, Simiao Ren<sup>1,3</sup>, Kin-Ping Wong<sup>3</sup>, Qingxiao Huo<sup>1</sup>, Chun-Sing Lee<sup>3</sup>, Yuen-Hong Tsang<sup>3</sup>, Yilong Han<sup>4</sup>, Chi-Hang Lam<sup>3\*</sup>

**Affiliations:**

<sup>1</sup>School of Science, Harbin Institute of Technology (Shenzhen), Shenzhen 518055, China

<sup>2</sup>Graduate School of Engineering, Nagoya Institute of Technology, Nagoya, 466-8555, Japan.

<sup>3</sup>Department of Applied Physics, Hong Kong Polytechnic University, Hung Hom, Hong Kong, China.

<sup>4</sup>Department of Physics, Hong Kong University of Science and Technology, Clear Water Bay, Hong Kong, China.

\*Correspondence to: E-mail: [C.H.Lam@polyu.edu.hk](mailto:C.H.Lam@polyu.edu.hk)

**This PDF file includes:**

Materials and Methods

Supplementary Results on Glassy Colloidal Systems

Supplementary Results on Glass-crystal Coexisting Systems

Figures S1 to S23



## 1. Materials and Methods

### 1.1. Experimental Colloidal Systems

We use polymethyl methacrylate (PMMA) colloidal particles for all of the experiments in this work. Each particle has a thin coating of trihydroxy octadecylsilane, which prevents them to stick together. We use two solutions of PMMA particles with average diameters  $\sigma_1 = 3.77\mu\text{m}$  and  $\sigma_2 = 4.62\mu\text{m}$ , as measured by the manufacturer. We write  $\sigma = \sigma_1 = 3.77\mu\text{m}$ , which is taken as the basic length scale in the following discussions. The diameter ratio of the two types of particles is  $\sigma_2/\sigma_1 \approx 1.23$ . To prepare the systems in the glassy state, we apply a bimodal (binary) mixture of these PMMA spheres to suppress crystallization. The mixture is equimolar with mole fractions  $x_1 \approx x_2 \approx 1/2$ . Alternatively, to study coexisting glassy and crystalline states, we use a unimodal system containing only the smaller particles, i.e.  $x_1 = 1$  and  $x_2 = 0$ .

In all experiments, particles are immersed in water and confined between the walls of thin transparent glass plates positioned horizontally. The particles fall under gravity onto the lower plate forming quasi-two-dimensional (2D) systems. Digital video microscopy measurements are made using an optical microscope with an oil immersion objective and a CCD camera mounted to the eyepiece. The number of particles within an optical image is typically around 1100. We are able to maintain practically all imaged particles within the depth of focus during the reported periods. Image-processing is performed using particle tracking codes from Ref.(31), which extract the trajectories of the centers of all imaged particles. The 2D particle packing fraction  $\phi$  is controlled via the initial particle density in the water solution and is measured from microscopic images. For the bimodal samples reported,  $\phi$  ranges from 0.70 to 0.80. To ensure equilibrium, we perform production measurements only after samples have been settled for at least 1, 3, and 8 days for  $\phi = 0.70\text{-}0.72$ ,  $0.73\text{-}0.76$  and  $0.78\text{-}0.80$ , respectively. Images are recorded at rates of one frame every 1, 2, 3 and 4s for  $\phi = 0.70$ ,  $0.72\text{-}0.74$ ,  $0.76$ , and  $0.78\text{-}0.80$ , respectively. To capture the slow dynamics at large  $\phi$ , we record images for durations up to  $10^6$  s. This amounts to more than 11 days of continuous imaging. It imposes technical challenges on data storage and particle trajectory analyses, which are overcome by appropriate software selection and minor modifications. Since our particles have relatively large sizes of  $3.77\mu\text{m}$  and  $4.62\mu\text{m}$ , all of them can be automatically identified in nearly all image frames.

A typical image of an experimental bimodal system is shown in Figure S1(a). Figure S1(b) shows the measured probability density function of the particle diameters. Typical particle configurations of experimental and simulated systems with packing fraction of 0.80 are shown in Figure S2.

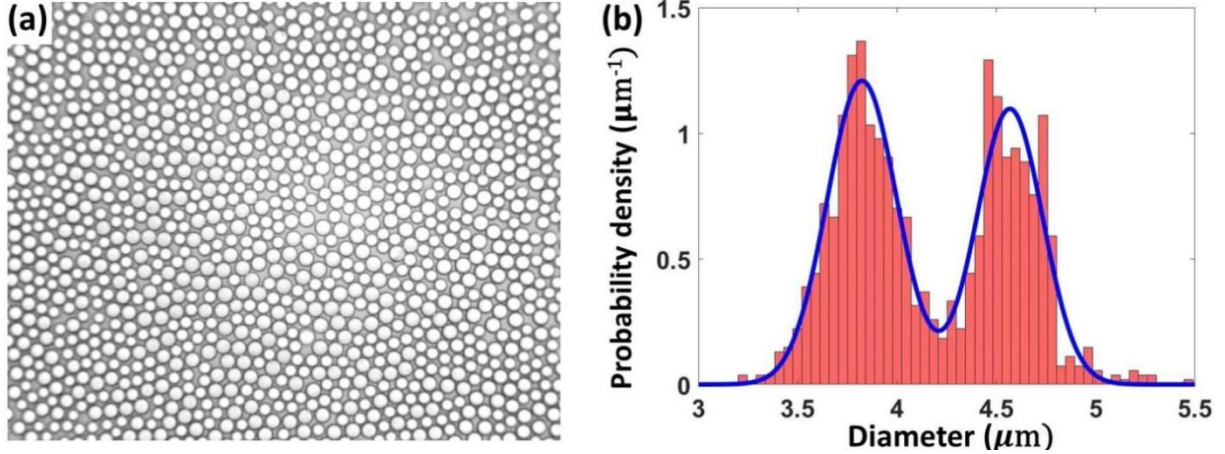


**Figure S1. Experimental Results:** (a) A typical optical image of a bimodal colloidal system. (b) Probability density function of particle diameters in the bimodal system. The fitted function (blue curve) is the sum of two Gaussians.

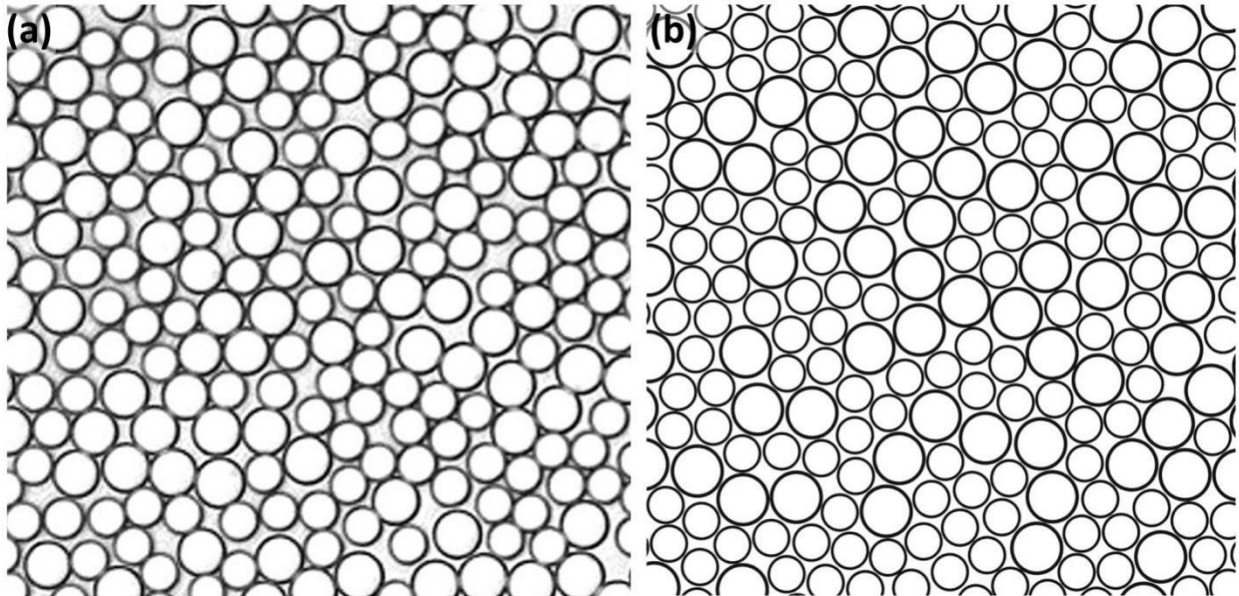


**Figure S2. Experimental and Simulation Results:** (a) An optical image of a bimodal colloidal system at packing fraction  $\phi = 0.80$  and (b) a computer simulated bimodal system also at packing fraction  $\phi_{MD} = 0.80$ .

## 1.2. Molecular Dynamics Simulations

To verify our experimental observations, we perform molecular dynamics (MD) simulations of glassy colloidal systems in 2D. The systems simulated are the same as those in Ref.(13). We adopt non-equimolar binary mixture systems consisting of  $N$  hard disks, where  $N = 64^2 = 4,096$ . The mole fractions of small and large disks with diameter of  $\sigma_1 = \sigma$  and  $\sigma_2 = 1.4\sigma$  are taken as  $x_1 = 2/3$  and  $x_2 = 1/3$  respectively. These conditions have been found to best suppress crystallization (13). The disks are placed in a  $L \times L$  square periodic boundary box, so that the packing fraction



is defined by  $\phi_{\text{MD}} = N\pi(x_1\sigma_1^2 + x_2\sigma_2^2)/4L^2$ . In this system,  $\phi_{\text{MD}}$  is the primary control parameter and it is varied from 0.72 to 0.81. The onset packing fraction between liquid and super-compressed liquids is  $\phi_{\text{MD}} \approx 0.76$ . The basic units of the system are length  $\sigma = 1$ , particle mass  $m = 1$  and inverse temperature  $\beta = 1/k_B T = 1$ . The systems are carefully prepared as pure amorphous state even at high  $\phi_{\text{MD}}$  after long-time equilibrations by efficient event-chain Monte Carlo (ECMC) calculations with up to  $O(10^{13})$  collisions (32). After equilibration, production runs for extracting particle trajectories are done using Event-Driven MD (EDMD) simulations (33).

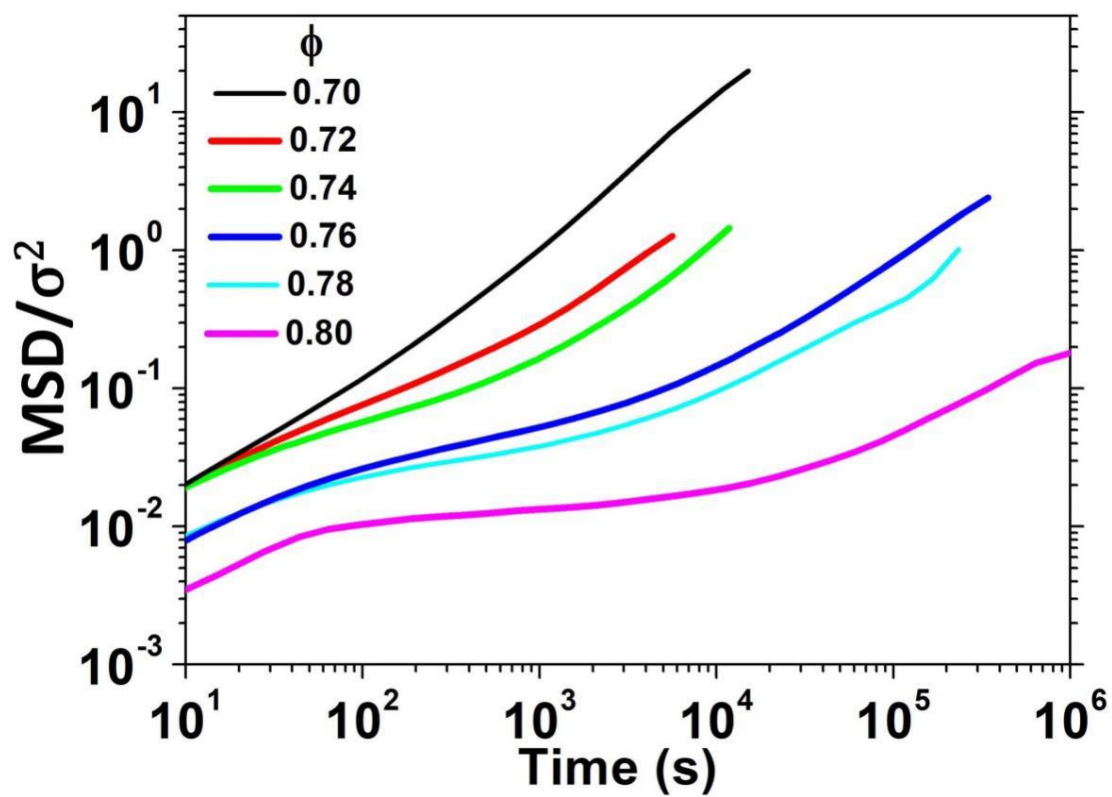
## 2. Supplementary Results on Glassy Colloidal Systems

### 2.1 Mean Square Displacement (MSD) and Comparing Experiments with Simulations

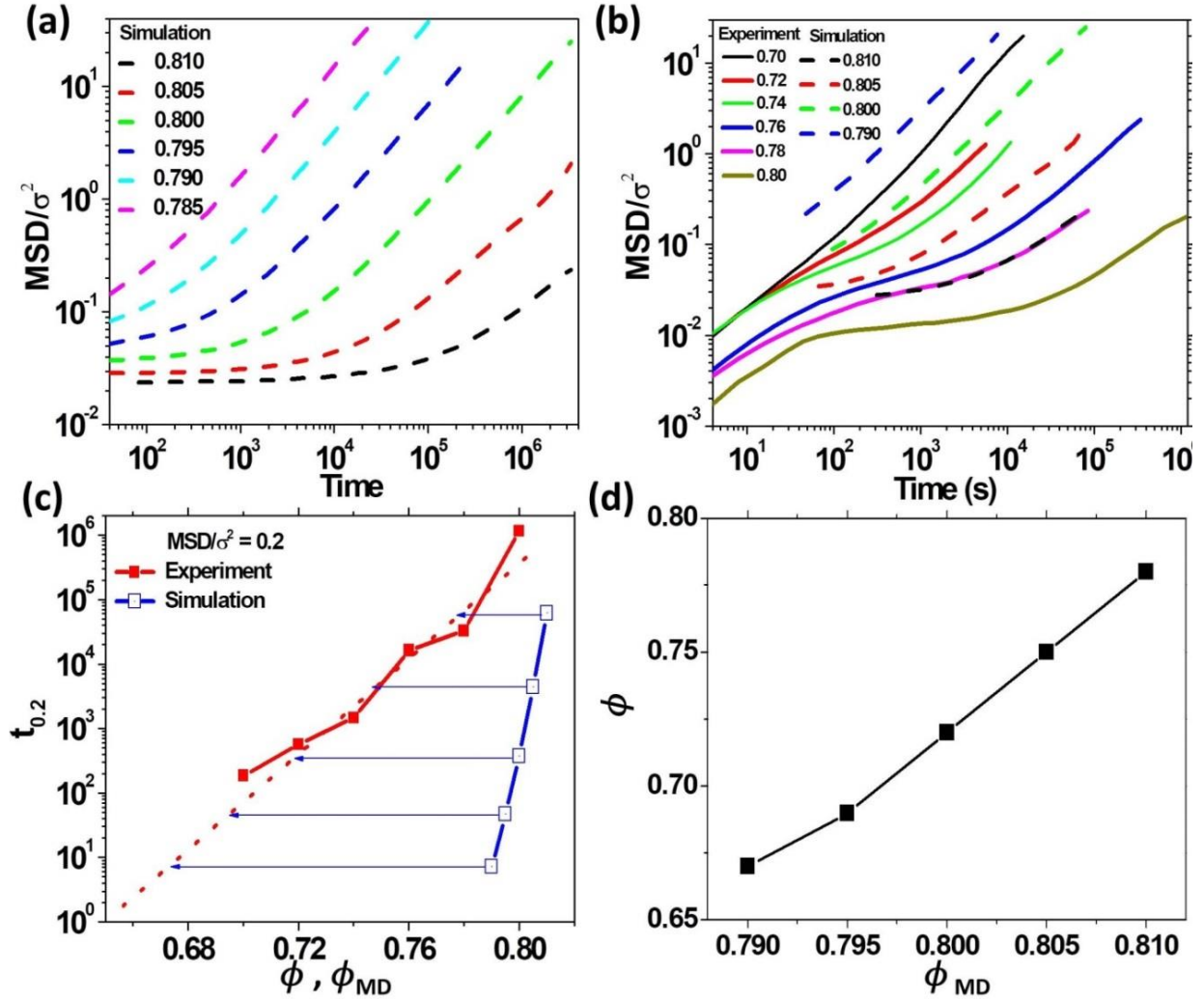
The measured particle mean square displacement (MSD) for various packing fraction  $\phi$  is shown in Figure S3. Very long imaging times have been applied at large  $\phi$  to ensure that the MSD have clearly evolved beyond the plateau values. This is important for assessing dynamics dominated by structural relaxations rather than localized vibrations.

Figure S4(a) shows our simulation results on the MSD. Despite exhibiting similar trends as in the experimental results, there are quantitative differences. The simulations show a much stronger dependence of the MSD on  $\phi_{\text{MD}}$  with a more dramatic slowdown as  $\phi_{\text{MD}}$  increases. The discrepancies may mainly be due to the effectively softer nature of the experimental particles resulting from the quasi-2D setup, in contrast to the genuine 2D systems of perfectly hard particles. Specifically, larger particles stand taller than smaller ones as they all rest under gravity on the lower glass plate. They may be momentarily squeezed slightly upward in crowded situations, and this creates additional free volumes for particles to move around. The kinetic arrest may thus be more stretched out with respect to  $\phi_{\text{MD}}$ . The finite rigidity of the experimental particles may also contribute to the softness. There are also other factors forbidding the direct comparison of  $\phi$  and  $\phi_{\text{MD}}$  in experiments and simulations. These include the slightly different particle radius distributions and mode fractions of the large versus small particles, which have been independently chosen to best suppress crystallization in the respective systems.

To enable qualitative comparisons between experiments and simulations, we apply an empirical multiplication factor of 0.025s to map the simulation time unit to physical time. Then, the experimental and simulation results follow a consistent trend as shown in Figure S4(b). For each packing fraction, we next find the time  $t_{0.2}$  at which the  $\text{MSD} = 0.2\sigma^2$ . A plot of  $t_{0.2}$  against  $\phi$  and  $\phi_{\text{MD}}$  is shown in Figure S4(c). The experimental data of  $t_{0.2}$  is fitted to a linear function in the semi-log scale as a first approximation. Finally, for each simulated packing fraction  $\phi_{\text{MD}}$ , the corresponding value of  $\phi$  is chosen as the one which provides the same value of  $t_{0.2}$  according to the fitted line. Figure S4(d) plots the mapped value of  $\phi$  as a function of  $\phi_{\text{MD}}$  hence obtained.



**Figure S3. Experimental Results:** Particle mean square displacement (MSD) against time for various packing fraction  $\phi$ .



**Figure S4. Experimental and Simulation Results:** (a) MSD against time from simulations. (b) MSD against time from experiments and simulations. (c) A plot of  $t_{0.2}$  versus  $\phi$  and  $\phi_{\text{MD}}$  from experiments and simulations, where  $t_{0.2}$  is the time to attain a MSD of  $0.2\sigma^2$ . The blue arrows show the mapping of  $\phi_{\text{MD}}$  to  $\phi$ . Note that time in simulations in (b) and (c) have been converted to physical units using an empirical factor of 0.025s. (d) Mapping of packing fraction from  $\phi_{\text{MD}}$  to  $\phi$ .

## 2.2. Particle Displacement Distribution, Particle Hops and Coarse-grained Trajectories

We now study the displacement  $\Delta r_i^c = |\vec{r}_i^c(t) - \vec{r}_i^c(0)|$  of each particle over time  $t$  based on instantaneous particle position  $\vec{r}_i^c(t)$ . Figure S5 shows the probability density function  $P(\Delta r/\sigma)$  of the normalized displacement  $\Delta r/\sigma$  averaged over particles and different definitions of time 0. Note that  $P(\Delta r/\sigma)$  is proportional to the van Hove correlation function. At small  $t$ , we observe a single-peaked function. As  $t$  increases, a secondary peak emerges at  $\Delta r \approx 1.2\sigma$ , representing activated hopping events. The peaks are separated by a dip at  $\Delta r \approx 0.8\sigma$ , which we take as the threshold of hopping. As shown in Figure S6, simulations show very similar behaviors.



The detailed dynamics during a particle hop can be illustrated by the normalized displacement  $\Delta r/\sigma$  plotted against time  $t$  during a hopping event and the hopping dynamics at  $\phi = 0.80$  is shown in Figure S7. The step-like increase in  $\Delta r/\sigma$  signifies a hop. The sudden rise takes a time, called the instanton time (12), to complete, which is about 200s in this example. Figure S8 shows a similar result from simulations at  $\phi_{MD} = 0.810$ , in which the instanton time is about 2000. Further analyses of particle dynamics are based on coarse-grained particle positions defined by  $\vec{r}_i^c(t) = \langle \vec{r}_i(t') \rangle_{t' \in [t, t + \Delta t_c]}$ , as already explained in the main text. Figure S9(a)-(d) show coarse-grained particle trajectories for the example of  $\phi = 0.76$ . Each trajectory is generated by joining time sequences of coarse-grained positions  $\vec{r}_i^c(t)$  at  $t = 0, \Delta t_c, 2\Delta t_c, \dots, T_{traj}$ . For small  $T_{traj}$  and  $\Delta t_c$ , considered in Figure S9(a), particles show small displacements in general. As both  $T_{traj}$  and  $\Delta t_c$  increase in Figures S9(b)-(d), many of the small displacements are increasingly averaged out, but some others reach lengths of order  $\sigma$  and represent string-like hopping motions. An extraordinarily high mobility contrast between particles is observed in Figure S9(d), indicating that hopping motions dominate the dynamics.

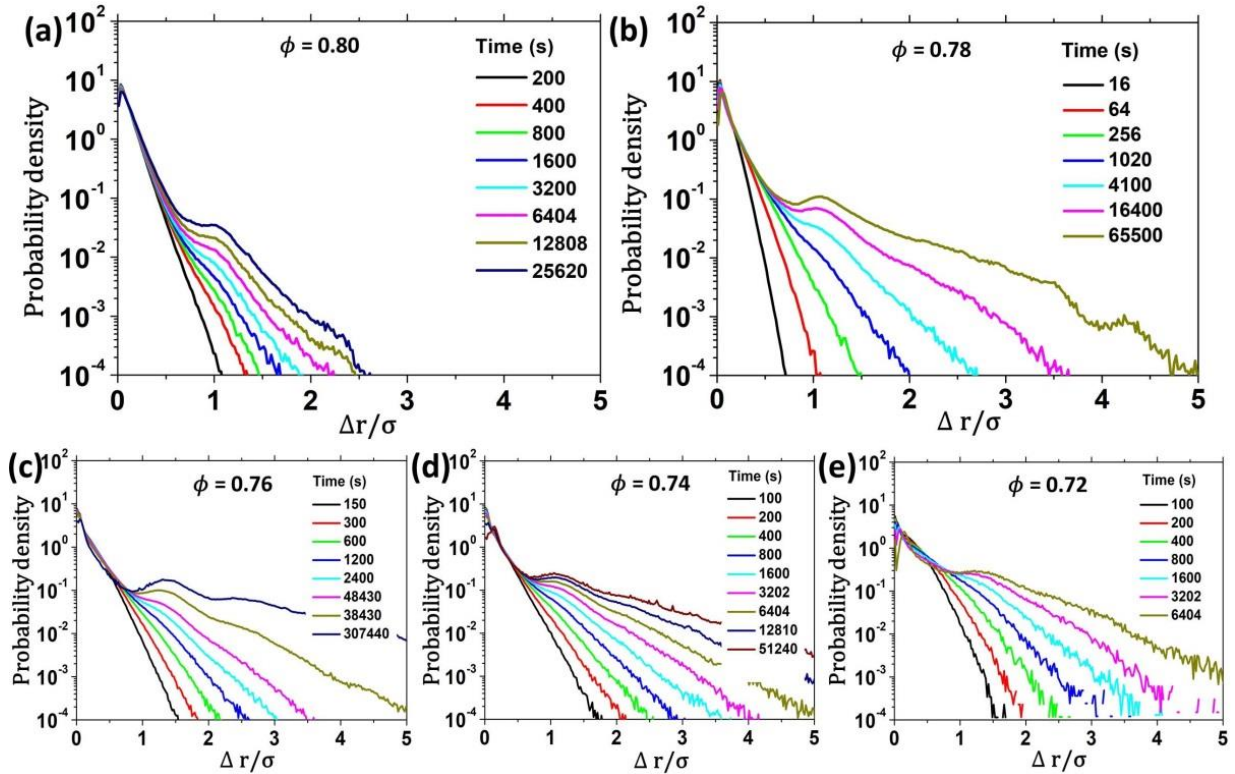


**Figure S5. Experimental Results:** Probability density function of particle displacement  $\Delta r$  in unit of  $\sigma$  based on instantaneous particle positions for packing fraction (a)  $\phi = 0.80$ , (b) 0.78, (c) 0.76, (d) 0.74, and (e) 0.72. In each case, a peak emerges at  $\Delta r \approx 1.2\sigma$  and an accompanying dip appears at  $\Delta r \approx 0.8\sigma$  as time  $t$  increases.

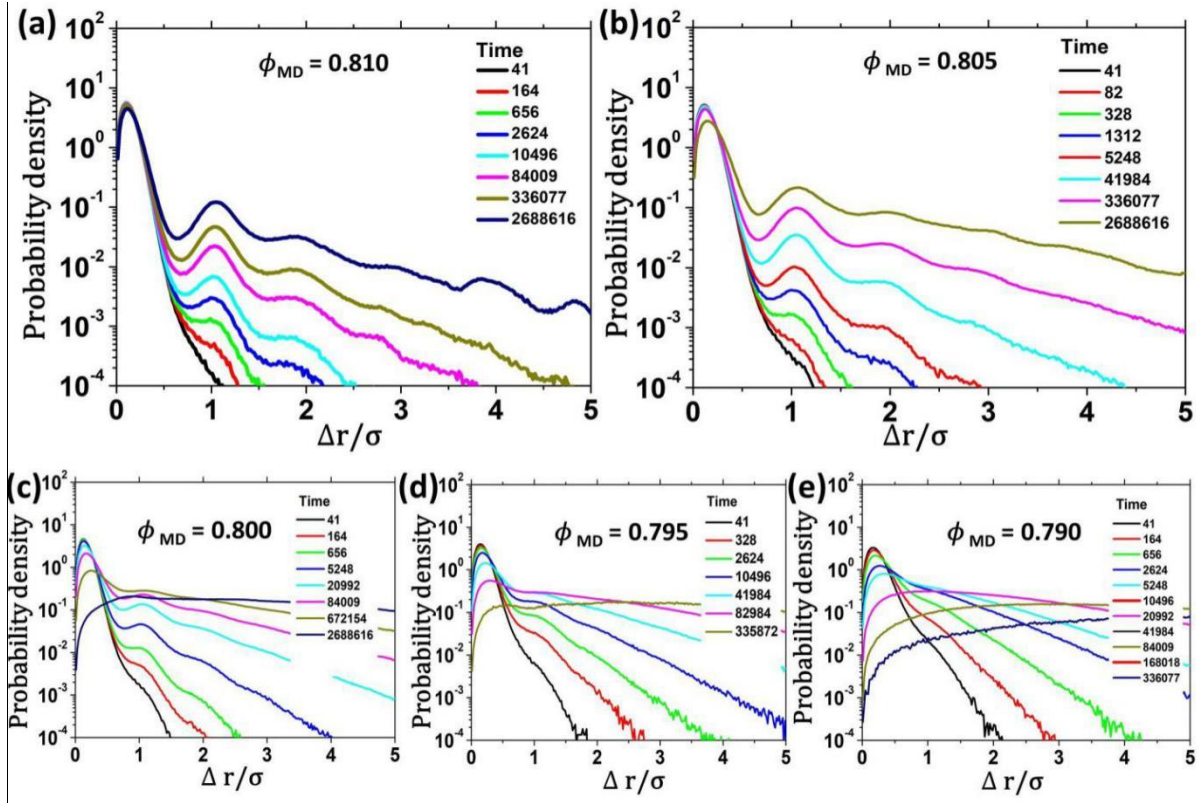


**Figure S6. Simulation Results:** Probability density function of particle displacement  $\Delta r$  in unit of  $\sigma$  based on instantaneous particle positions for packing fraction (a)  $\phi_{MD} = 0.810$ , (b) 0.805, (c) 0.800, (d) 0.795, and (e) 0.790.

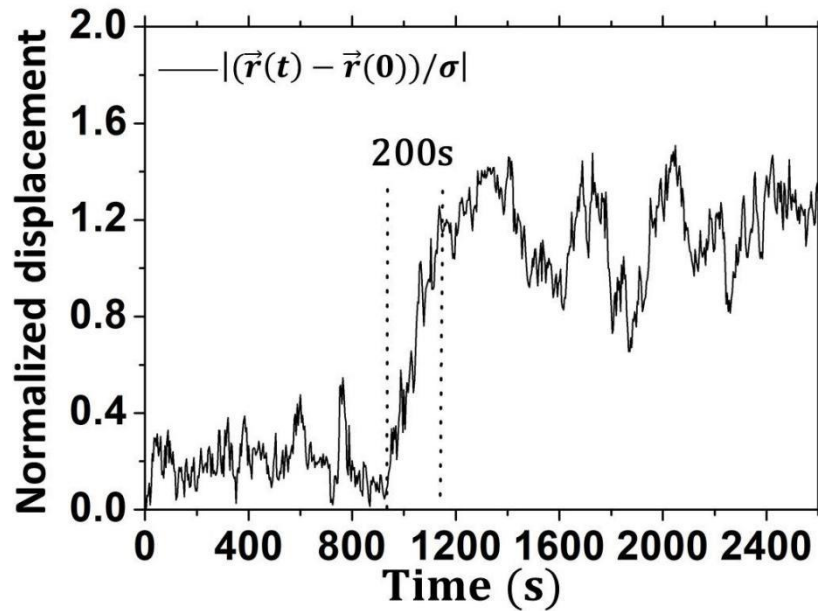


**Figure S7. Experimental Results:** Particle displacement  $\Delta r$  in unit of  $\sigma$  against time  $t$  based on instantaneous particle positions during a hopping event for  $\phi = 0.80$ . The instanton time is about 200s. The particle vibrates around metastable states before and after the hop.

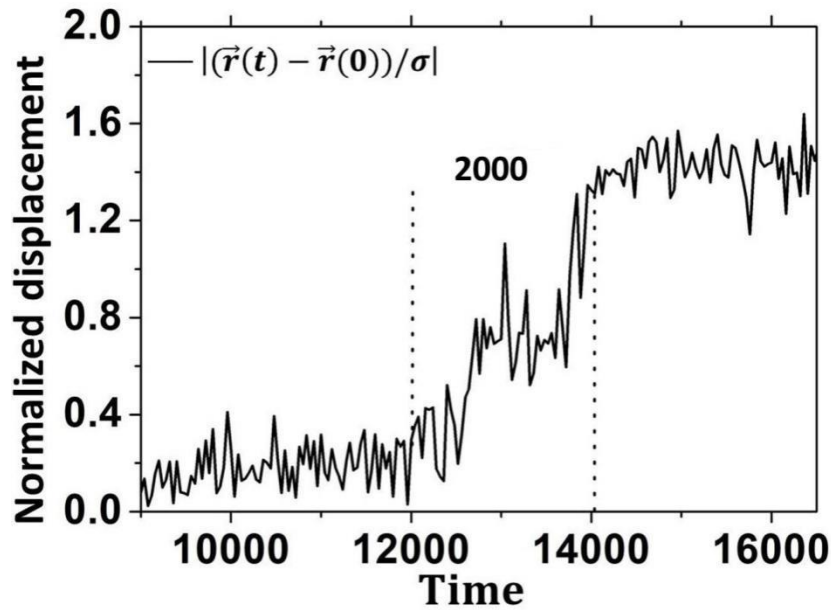


**Figure S8. Simulation Results:** Particle displacement  $\Delta r$  in unit of  $\sigma$  against time  $t$  based on instantaneous particle positions during a hopping event for  $\phi_{MD} = 0.810$ . The instanton time is about 2000.



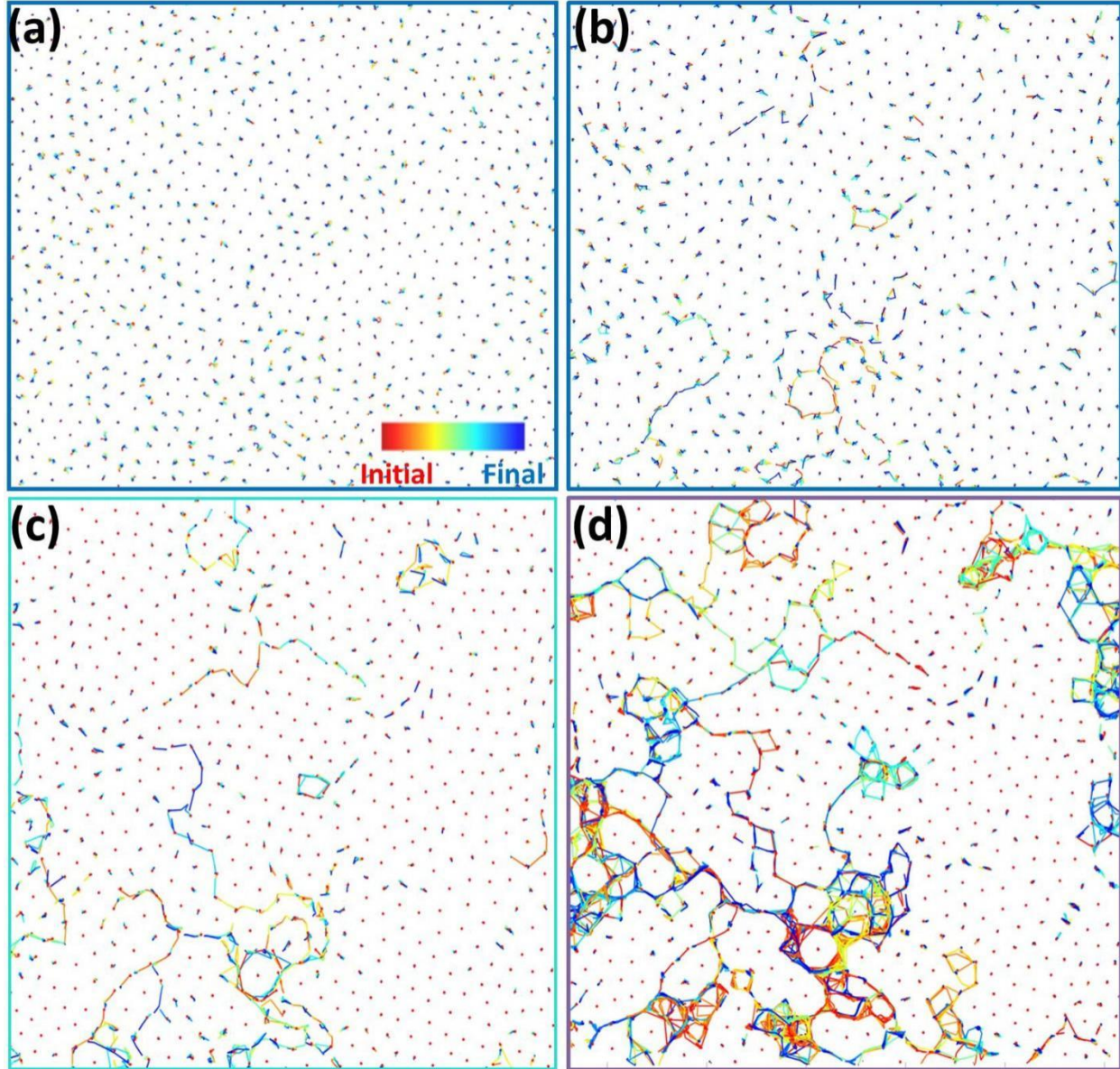


**Figure S9. Experimental Results:** Time-colored coarse-grained particle trajectories at  $\phi = 0.76$ . Each trajectory is represented by line segments joining consecutive coarse-grained particle positions. We take **(a)**  $T_{traj} = 600$  s,  $\Delta t_c = 8$  s **(b)**  $T_{traj} = 1200$ s,  $\Delta t_c = 120$ s, **(c)**  $T_{traj} = 18000$ s,  $\Delta t_c = 900$ s and **(d)**  $T_{traj} = 350000$ s,  $\Delta t_c = 1750$ s, where  $T_{traj}$  is the time duration covered by a whole trajectory and  $\Delta t_c$  is the time interval during which a coarse-grained particle position is averaged over. Line segments are colored according to time from red to blue, following Figure 1(a) of the main text. Initial particle positions are denoted by red dots.

### 2.3. String-like motions and quasi-voids

We have illustrated string-like motions and quasi-void dynamics in Figs. 1 and 2 in the main text based on particle trajectories and configurations extracted from optical images using particle identification and tracking software. To confirm that our conclusions are not artifacts of these sophisticated analysis methods, we now examine the optical images more directly using a simple image compositing approach.

Figure S10(a)-(b) shows optical images of our experimental colloidal system before and after the string-like motion in Fig. 1(b)-(c) in the main text. We have colored those particles related to the motion for easier identification. Free volumes can be understood as spaces available throughout the system for inserting a new particle (34). The fragmented free volumes constituting the quasi-void being transported are illustrated as the blue areas. The particle configurations observed in the optical images in Fig. S10(a)-(b) is fully consistent with the computer regenerated images in Fig. 1(b)-(c) based on tracked particle positions.

Figure S10(c) shows a composite optical image clearly illustrating the particle movements. It is essentially a time-averaged optical image of the initial configuration put on top of a time-averaged image of the final configuration, after the latter has been converted to cyan. Only simple pixel-wise image processing operations are used. Specifically, the initial (final) image is obtained by averaging over the red-green-blue (RGB) values of 8 time-consecutive images before (after) the string-like motion. Let  $(r^I, g^I, b^I)$  and  $(r^F, g^F, b^F)$  be the RGB values of a pixel in the initial and final averaged images respectively. The corresponding pixel in Fig. S10(c) is then assigned an RGB value of  $\max\{(r^I, g^I, b^I), (0, g^F, b^F)\}$ . The maximum operation ensures that a white pixel dominates over a colored one of the same intensity and hence provides the perception of being on top. Similarly, Fig. S10(d) shows the final image on top of the initial one which is converted to red. Technically, the pixel value is calculated by  $\max\{(r^I, 0, 0), (r^F, g^F, b^F)\}$ .

We reproduce Fig. S10(c)-(d) in Fig. S10(e)-(f) with added annotations, including blue arrows showing the displacements of the relevant particles. In Fig. S10(e), a region close to the string tail, as defined in the main text, is illustrated by a yellow dotted line. The region initially holds four particles. During the string-like motion, a particle (the big purple particle in Fig. S10(a)) moves by a distance comparable to its diameter and enters the region nearly completely. The region thus finally holds five particles. Since we consider a high packing fraction, the region must initially possess a higher than average amount of free volumes, which can clearly be observed in Figs. S10(a), (c) and (e). We have defined the quasi-void as the free volumes which allow for this extra particle in the region and are shaded schematically in blue in Fig. S10(a). Similarly, from Fig. S10(f), a particle (the orange particle in Fig. S10(a)) exits the region marked by the dotted yellow line. The region originally holding four particles is then left with only three. Equivalently, one quasi-void resides in the region in the final configuration as indicated by the blue areas in Fig. S10(b).

As exemplified in Fig. S10, a string-like motion in general involves a number of particles internal to the string with displacements close to the average particle diameter (i.e.  $1.12\sigma$  in our colloidal system) and displaces the preceding particles nearly completely. In addition, there is also a tail region which loses a quasi-void and a head region which gains a quasi-void.

We adopt explicit rules to define the free-volume fragments in a quasi-void, based on a particle push-off process. Figure S11 illustrates the rules schematically for the simplified case of a one-dimensional arrangement of particles with a uniform radius  $\sigma$  close to the string head. In this definition, the center of the quasi-void is located at the center of the final position of the particle at the string head. The effective quasi-void area is the invaded area of the string head, after other particles are pushed-off. It equals about 90% of the area of the particle at the string head, which may be a large or small particle. The free-volume gain from pushing off a particle dictates the geometries of the free-volume fragments to be iteratively included in the quasi-void.

It can be straightforwardly generalized to 2D in which the fragments are not only translated but also rotated by the angle between the displacement vectors of the pushing and pushed particles. In addition, a linear sequence of pushing off may become a branched process. With the above definition, the quasi-void can be objectively identified.

Similar dynamics is observed in our MD simulations. Figure S12 shows a typical string-like motion at  $\phi_{\text{MD}} = 0.810$ , which is the highest packing fraction simulated in this work. We have also illustrated schematically the fragmented free volumes of a quasi-void which are transported by the string-like motion from one end to the other end of the string.

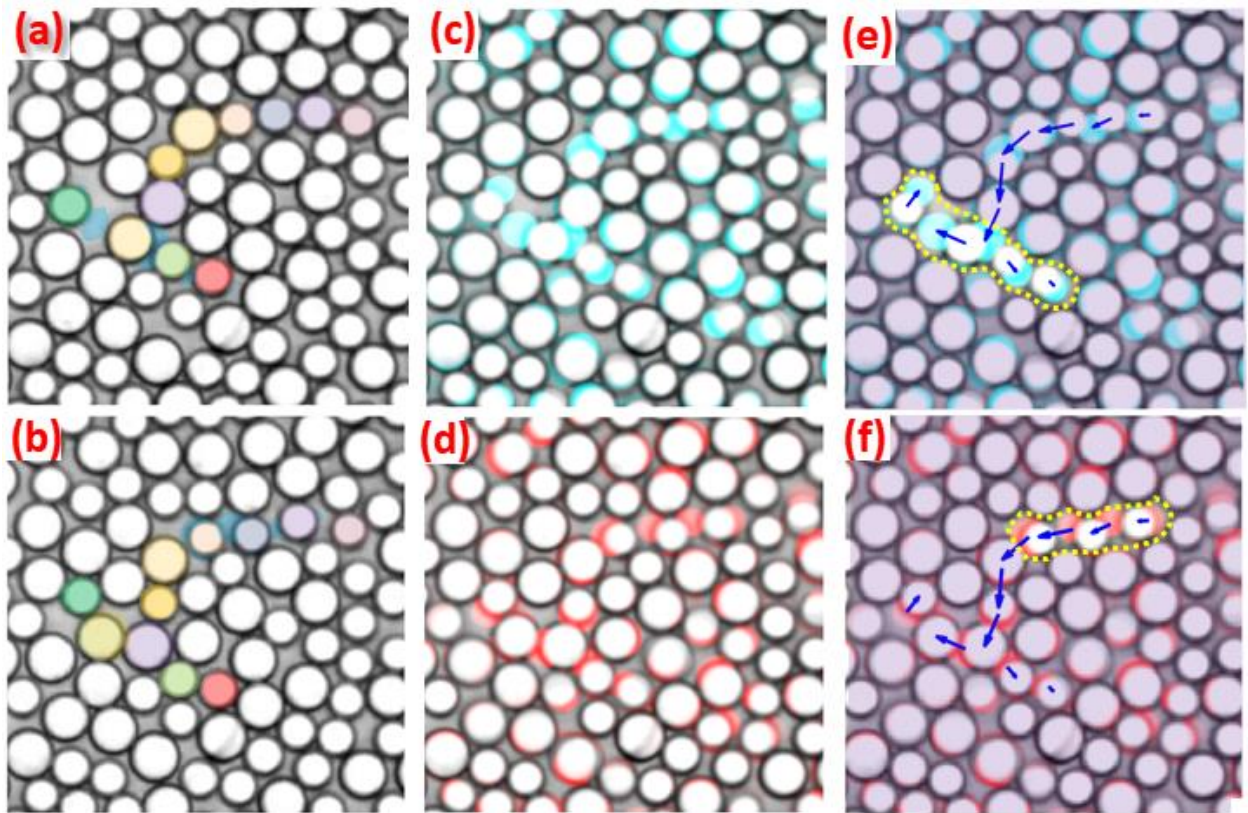


**Figure S10. Experimental results:** (a)-(b) Optical images showing initial (a) and final (b) particle configurations before and after a string-like motion. The same motion is also illustrated in the computer regenerated images in Figure 1(b) and (c) in the main text. Particles involved in the motion are colored for easier identification. The fragmented free volumes constituting the quasi-void being transported are illustrated as blue areas. (c) A composite optical image with initial particle configuration (white) shown ‘on top of’ the final configuration (blue). The initial



and final images used are each averaged over 8 raw images to suppress effects of vibrations. **(d)** A composite optical image similar to (c) with final particle configurations (white) shown ‘on top of’ the initial configuration. **(e)** The same composite image in (c). A region (yellow dotted line) initially contains 4 particles and one quasi-void but finally holds 5 particles. Displacements of particles related to the string-like motion are illustrated by blue arrows. **(f)** The same composite image in (d) illustrating a region (yellow dotted line) holding 4 particles initially in contrast to 3 particles and one quasi-void finally.

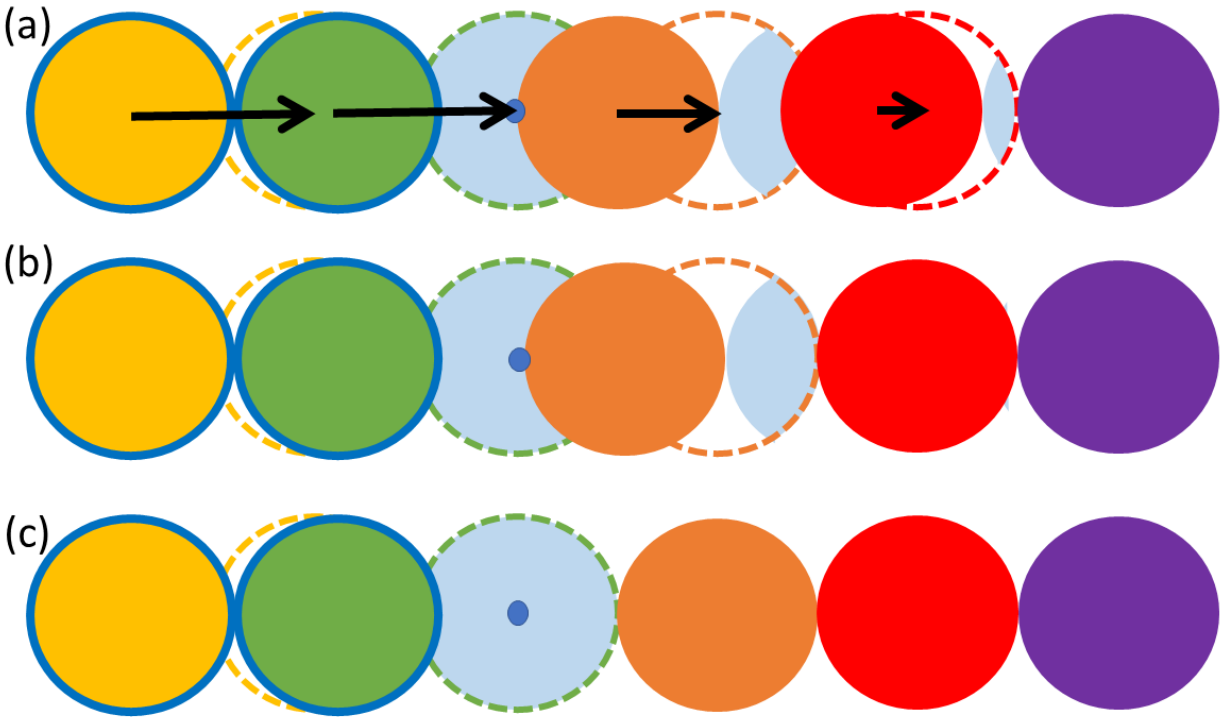


**Figure S11.** (a) Schematic diagram of initial (solid spheres) and final (open spheres) configurations of particles close to the head of a string-like motion. Their displacements are indicated as black arrows. The green and yellow particles has large displacements ( $> 0.8\sigma$ ) and take part in a string-like motion, which also induces smaller displacements of the orange and red particles. The green particle located at the invading end of the string is defined as the string head. The quasi-void transported by the string is defined as consisting of three free-volume fragments (blue areas). Its position is defined for simplicity as the center of the final position of the string head (blue dot), which may or may not be occupied by a particle initially. The string head is able to move to its final position because particles in front (orange and red) are sequentially pushed off, a process transporting and effectively reassembling the required free volume fragments. (b) To schematically reassemble the fragments, the right fragment is first transported by the movement of the red particle to combine with the middle fragment. (b) The combined fragment is further transported by the movement of the orange particle to combine with the main fragment on the left. (c) The fragments have been constructed so that the reassembled free volume coincides with the invaded volume by the string head. Note however that particles in general move simultaneously and configurations in (b) and (c) are for illustration only.

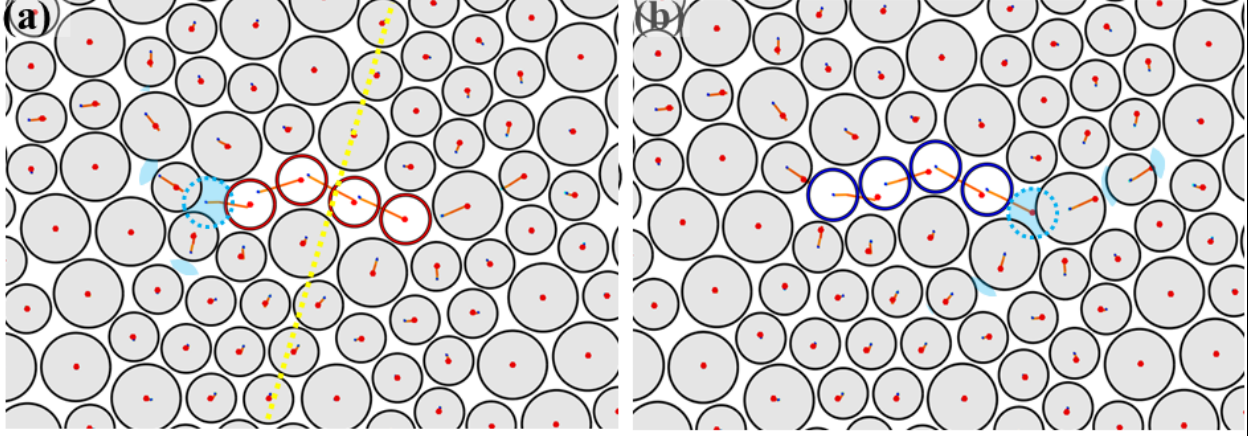


**Figure S12. Simulation Results:** (a) and (b) Coarse-grained trajectories for duration  $T_{\text{traj}} = 20$  showing a typical string-like particle hopping motion at packing fraction  $\phi_{\text{MD}} = 0.810$ . Particle configurations at the beginning (a) and the end (b) of the period are also shown. A quasi-void consisting of fragmented free volumes (blue areas) is transported by the string across a line of otherwise nearly stationary particles (yellow dotted line). Note that the blue dotted circles show the final position of the particle at the string tail in (a) and the initial position of the particle at the string head in (b).

#### 2.4. Displacement Correlation and Particle Back-and-forth Hopping Motions

From coarse-grained particle trajectories at large  $\phi$ , we observe particle hops in a background of nearly stationary particles. This is in sharp contrast to typical collective flow in non-glassy liquids in which particles tend to move with stronger local correlations. To quantify this high mobility contrast in the glassy phase, we have defined a displacement correlation  $Y$  in Eq. (1) in the main text which is reproduced here as:

$$Y = \langle \min\{\Delta r_j\}_{j \in \Omega_i} / \Delta r_i \rangle_{i \in \Omega_{\text{hop}}}.$$

In this formula,  $\Delta r_i = |\vec{r}_i^c(t + \delta t) - \vec{r}_i^c(t)|$  is the coarse-grained displacement of particle  $i$  over a duration  $\delta t$  at time  $t$ . We only consider particle  $i$  in the set  $\Omega_{\text{hop}}$  of hopped particles, satisfying  $\Delta r_i > 0.8\sigma$  with the threshold  $0.8\sigma$  corresponding to a dip in the van Hove correlation function (see Figure S5). We then examine the set  $\Omega_i$  of nearest neighbors of particle  $i$ , which is defined as its 6 nearest particles based on coarse-grained particle positions at time  $t$ . The correlation  $Y$  is the minimum value of the coarse-grained displacements  $\Delta r_j$  of these neighboring particles, after being normalized by  $\Delta r_i$ . We have averaged  $Y$  over all hopping particles  $i$  and time  $t$ . Under this definition, string-like motions should contribute little to  $Y$  because not all 6 neighboring particles participate in the string in general. Hence,  $Y$  measures mainly the magnitude of the collective flow component of the dynamics.

Figure S13(a) shows the results of  $Y$  against  $\phi$ . Coarsened particle positions  $\vec{r}_i^c$  are calculated by averaging instantaneous positions over an averaging time  $t_c = 10, 20, 30$  and  $40$ s for  $\phi = 0.70, 0.72-0.74, 0.76$  and  $0.78-0.80$ , respectively, which correspond to 10 recorded image frames in all cases. We have also taken  $\delta t \approx 400$ s for all values of  $\phi$ . This choice of  $\delta t$  is shorter than a typical

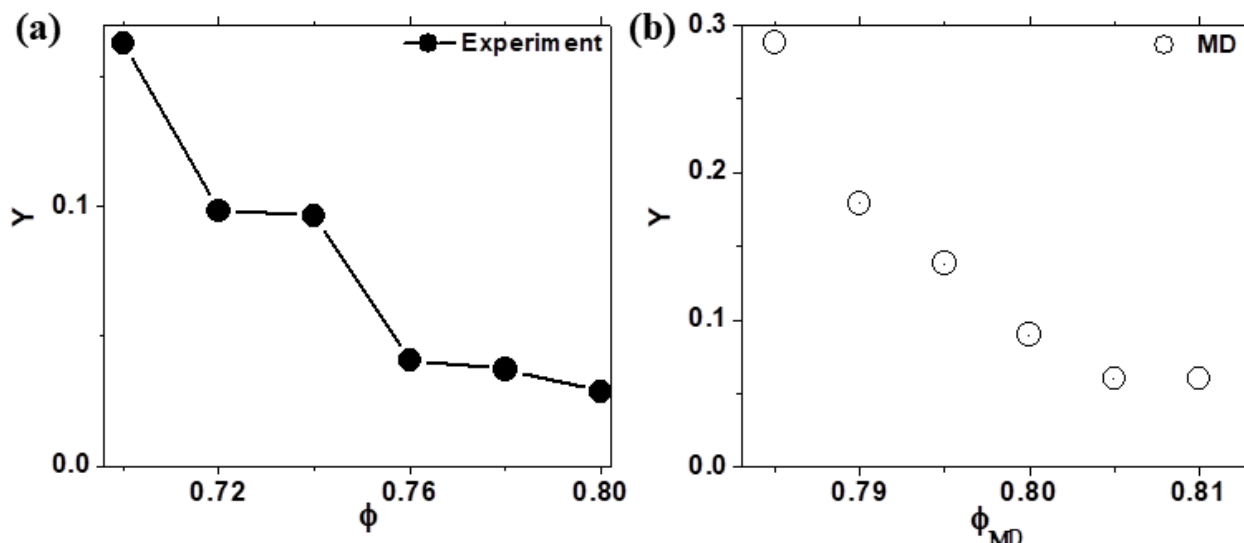
waiting time of a particle hop so that double hops within the duration are few. In addition, it is longer than the instanton time (see Sec. 2.2 in SI), which is the typical duration of the course of a hopping event. To illustrate particle motions under these coarsening parameters, Figure S14 shows examples of particle trajectories under these coarsening conditions. Similarly, Figure S13(b) shows results on  $Y$  from simulations, where we have taken  $\delta t = 67240$  and  $\Delta t_c = 1681$  for all values of  $\phi_{MD}$ . Corresponding coarse-grained trajectories from simulations are shown in Figure S15.

Figures S13(a-b) both show a similar trend of  $Y$  decreasing with  $\phi$ . For a quantitative comparison, we reparametrize  $\phi_{MD}$  to  $\phi$  based on the particle MSD measurements explained in Sec. 2.1 in SI. The results are shown in Figure 4(a) in the main text. The good quantitative agreement then obtained is non-trivial and shows that the simulations indeed closely model the experiments. The monotonic decrease of  $Y$  towards 0 in Figure 4(a) shows the diminishing role of collective flow as  $\phi$  increases. This supports the study of glassy dynamics based solely on hopping motions.

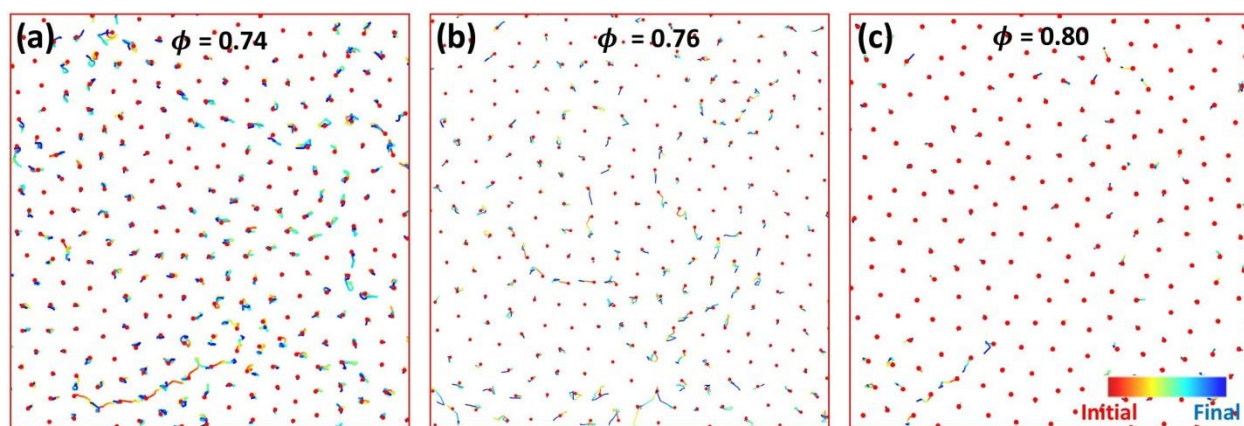
To quantify back-and-forth particle hops, we calculate the returning and escaping probabilities  $P_{ret}$  and  $P_{esc}$  of hopped particles. Using the same definitions of particle hops above, we monitor the further motions of particle  $i$  which has hopped during the period from  $t$  to  $t+\delta t$ . We examine its coarse-grained position  $\vec{r}_i^c(t')$  at later times  $t' = t + \delta t + n\Delta t_c$  ( $n = 1, 2, \dots$ ) up to  $t + \delta t + \tau_{max}$ . If it first returns to its original position, i.e.  $|\vec{r}_i^c(t') - \vec{r}_i^c(t)| < 0.4\sigma$ , the motion is referred to as a returning hop. Alternatively, if it first hops again to a third position, i.e.  $|\vec{r}_i^c(t') - \vec{r}_i^c(t + \delta t)| > 0.8\sigma$ , we classify it as an escaping hop. Otherwise, the particle is deemed stationary. The particle returning and escaping probabilities  $P_{ret}$  and  $P_{esc}$  are hence calculated.

Figure S16(a-b) shows the results on  $P_{ret}$  and  $P_{esc}$  for experiments and simulations. We have taken the same values of  $t_c$  and  $\delta t$  given above for the calculation of  $Y$ . For the experiments, we put  $\tau_{max} = 1000s, 6000s, 90000s, 96000s$  and  $360000s$  for  $\phi = 0.70-0.72, 0.74, 0.76, 0.78$  and  $0.80$  respectively. For the simulations,  $\tau_{max} = 1000, 2000, 6000$  and  $7000$  and  $8000$  for  $\phi_{MD} = 0.785-0.790, 0.795, 0.800, 0.805$  and  $0.810$  respectively. These values of  $\tau_{max}$  are large enough so that particles have returned or escaped in most cases resulting at  $P_{ret} + P_{esc} > 90\%$ .

Similar to the study of  $Y$  above, experimental and simulation results on  $P_{ret}$  and  $P_{esc}$  show consistent trends. Again, after reparametrizing  $\phi_{MD}$  to  $\phi$  based on the particle MSD, a good quantitative agreement is obtained as shown in Figure 4(b) in the main text. We have obtained from experiments a very high probability of  $P_{ret} \approx 0.80$  for returning events, which appears to further increase towards 1 as  $\phi$  increases. This shows the quantitative, and possibly, even qualitative importance of back-and-forth particle hopping motions. Such motions are observable directly from particle trajectories as shown in Figure S17.



**Figure S13. Experimental and Simulation Results:** Displacement correlation  $Y$  against packing fraction  $\phi$  and  $\phi_{MD}$  from (a) experiments and (b) simulations.



**Figure S14. Experimental Results:** Typical particle trajectories for coarsening parameters  $\delta t$  and  $\Delta t_c$  used in calculating  $Y$ ,  $P_{ret}$  and  $P_{esc}$  for  $\phi =$  (a) 0.74, (b) 0.76, and (c) 0.80.

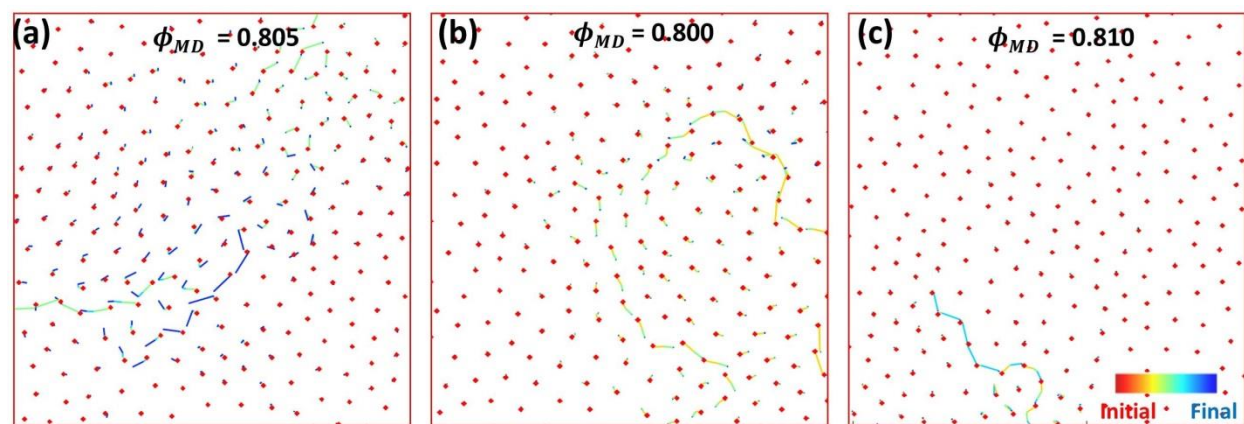


**Figure S15. Simulation Results:** Typical particle trajectories for coarsening parameters  $\delta t$  and  $\Delta t_c$  used in calculating  $Y$ ,  $P_{ret}$  and  $P_{esc}$  for  $\phi_{MD} =$  (a) 0.800, (b) 0.805, and (c) 0.810.



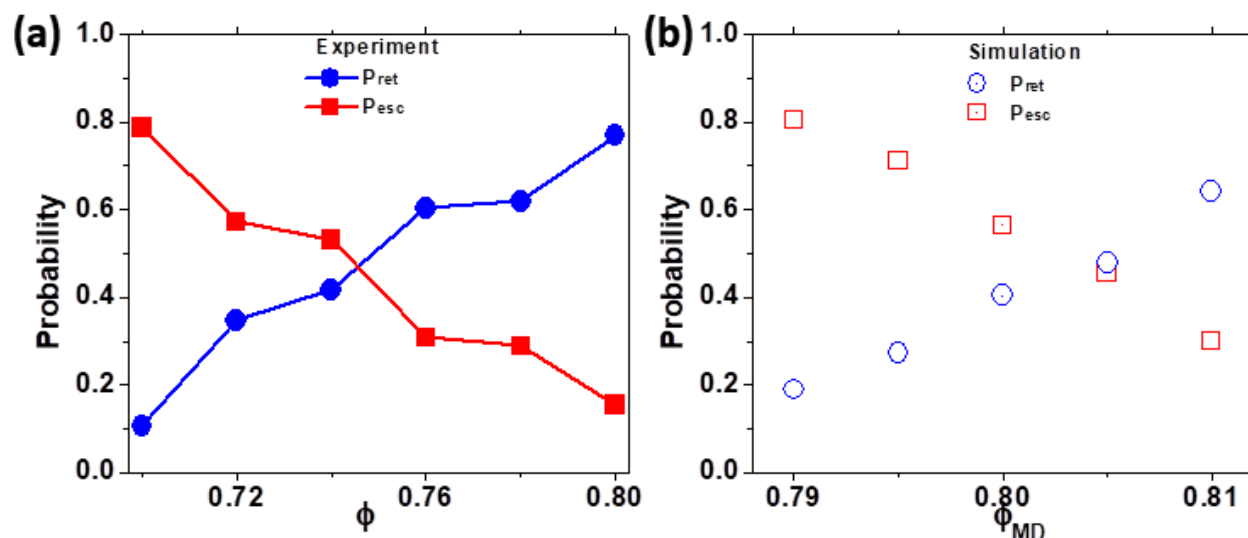


**Figure S16. Experimental and Simulation Results:** Returning and escaping probabilities  $P_{ret}$  and  $P_{esc}$  of hopped particles against packing fraction  $\phi$  and  $\phi_{MD}$  from (a) experiments and (b) simulations.

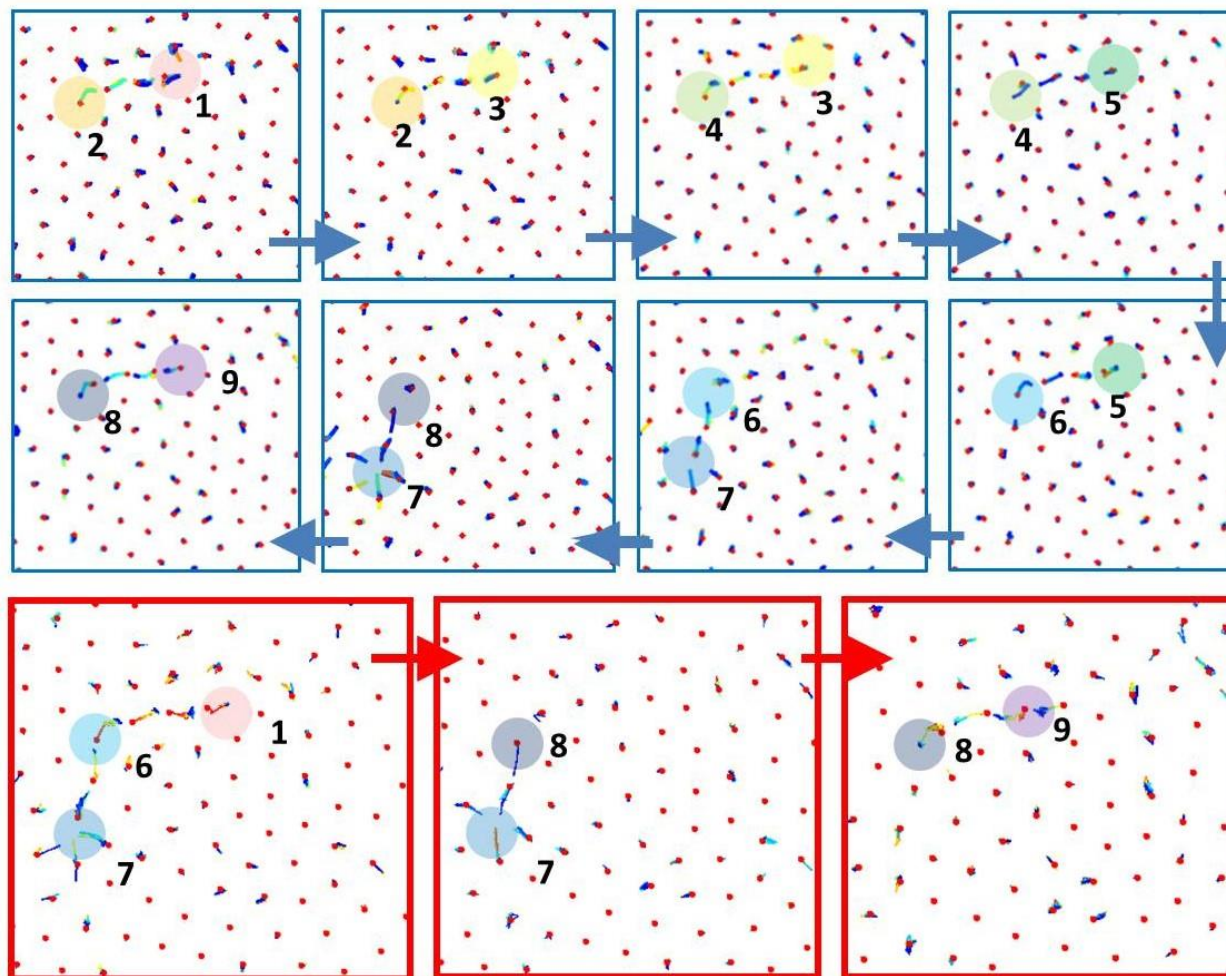


**Figure S17. Experimental Results:** Blue boxes: Consecutive time sequence of coarse-grained trajectories at  $\phi = 0.80$ . Numbered circles mark initial and final positions of a quasi-void. Many back-and-forth motions are observed. Red boxes: Consecutive time sequence of the same motions as in the blue boxes but at longer coarsening times. Some back-and-forth motions are hidden by the further coarsening.

## 2.5. String-like motions in mobile clusters

For each value of  $\phi$ , we show in Figure S18 particle trajectories over time  $T_{traj}$  so that particle  $\text{MSD} \approx 0.2\sigma^2$ . We identify the mobile particle group as the set of particles with coarse-grained displacements  $\Delta r_i^c = |\vec{r}_i^c(T_{traj}) - \vec{r}_i^c(0)|$  within the top 15% among all particles. Particles in the mobile group are represented by solid circles in Figure S18. Note that some particles exhibiting back-and-forth motions and having returned to the original positions are not considered mobile under this widely used definition. We further classify the mobile particles as core-like and string-like depending on the local neighboring conditions of the mobile particles following Ref (7). They are colored as red and blue respectively in Figure S18. Our results show a clear trend of a crossover from predominantly string-like to predominantly core-like mobile domains, in full agreement with the observation in Ref(7). In fact, an analogous crossover of the geometries of mobile particles is also observable from a lattice model of glass (see Figure. 7 of Ref(20)).

We have shown in Figure 3 of the main text particle trajectories in a cluster of core-like particles. Detailed trajectories show that particle motions are indeed composed of two sequences of string-like motions induced by two quasi-voids. As further examples, detailed dynamics in three core-like clusters Figure S18(c) are illustrated in Figures S19-S21. They similarly show sequences of string-like motions. Similarly, Figures S22 shows trajectories in a core-like cluster from simulations broken down into sequences of string-like motions.

All these examples show that particle dynamics are dominated by string-like motions induced by quasi-voids even at a large  $\phi$  for both string-like and core-like clusters, despite apparently different cluster geometries. The compact core-like geometries in fact result from the increased dynamic heterogeneity at large  $\phi$ , meaning that particle hops recur again and again at highly localized regions so that strings superimpose each other to form compact clusters. The string dominated dynamics are otherwise similar to those in string-like clusters and at smaller values of  $\phi$ . We have studied trajectories covering durations  $T_{traj}$  at which the  $\text{MSD} \approx 0.2\sigma^2$ . We take  $T_{traj} = 360\text{s}$ ,  $15000\text{s}$  and  $1000000\text{s}$  for  $\phi = 0.72$ ,  $0.76$  and  $0.80$  respectively. The top 15% mobile particles are found to have displacements  $\Delta r_i$  beyond  $0.33\sigma$ ,  $0.27\sigma$  and  $0.42\sigma$  respectively, which should be large enough to exclude most vibrations, despite being smaller than our threshold  $0.8\sigma$  of hopping used above. We emphasize that these conditions are important to observe true glassy dynamics as they ensure the dominant role of structure relaxations as opposed to vibrations.

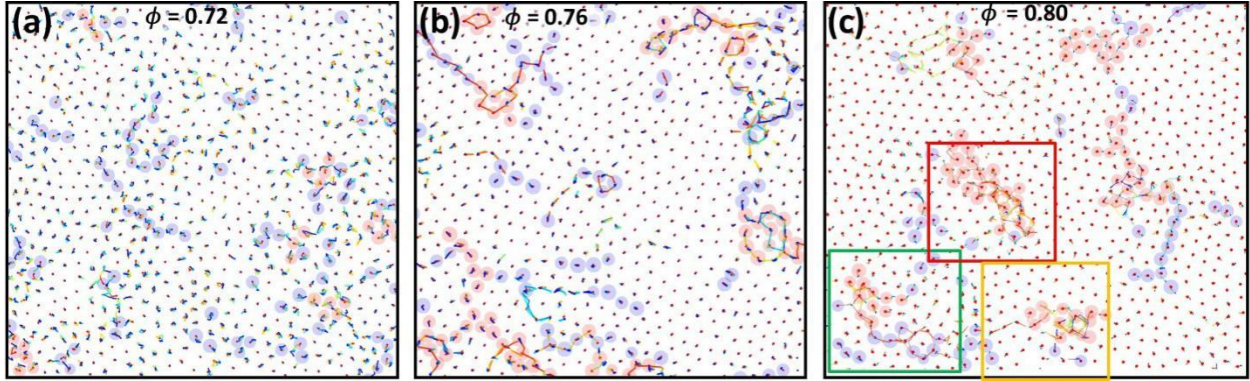


**Figure S18. Experimental Results:** Particle trajectories for duration  $T_{traj}$  so that the  $MSD \approx 0.2\sigma^2$  for (a)  $\phi = 0.72$ , (b) 0.76, and (c) 0.80. The top 15% most mobile particles based on their displacements are shown as circles. Mobile particles classified core-like and string-like are shaded in red and blue respectively.

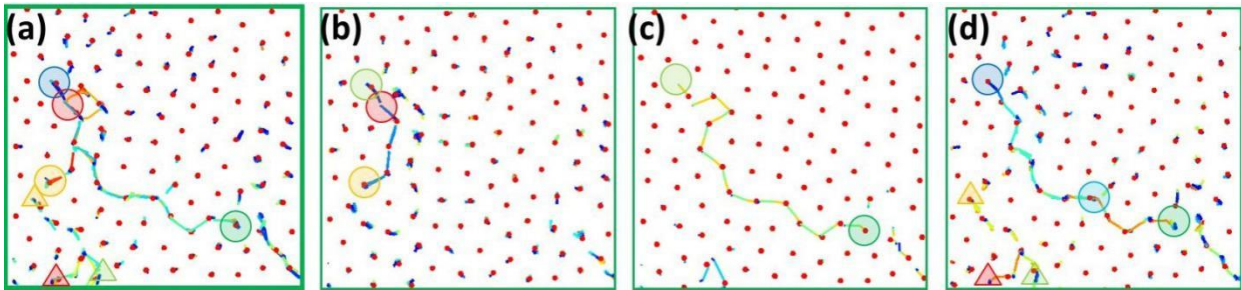


**Figure S19. Experimental Results:** (a) Coarse-grained trajectories from the green box in Figure S18 (c). (b)-(d) Consecutive time sequence of coarse-grained trajectories showing details of the dynamics in (a) containing a core-like mobile group. The motions are induced by two quasi-voids denoted by colored circles and triangles.

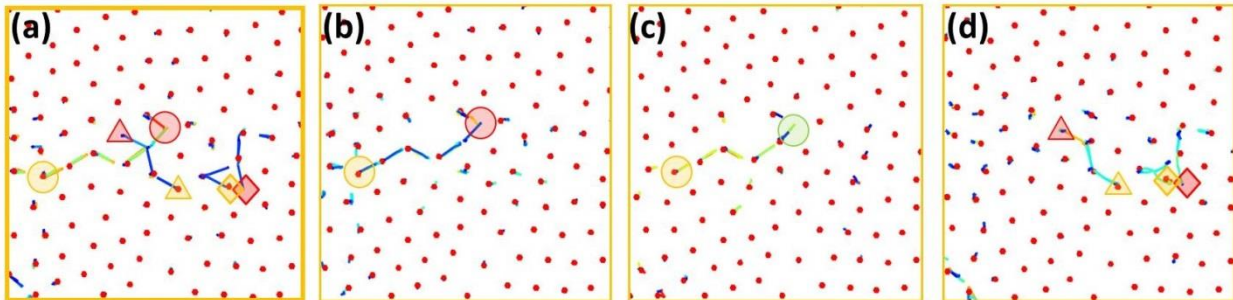


**Figure S20. Experimental Results:** (a) Coarse-grained trajectories from the orange box in Figure S18 (c). (b)-(d) Consecutive time sequence of coarse-grained trajectories showing details of the dynamics in (a) containing a core-like mobile group. The motions are induced by three quasi-voids denoted by colored circles, triangles and diamonds.



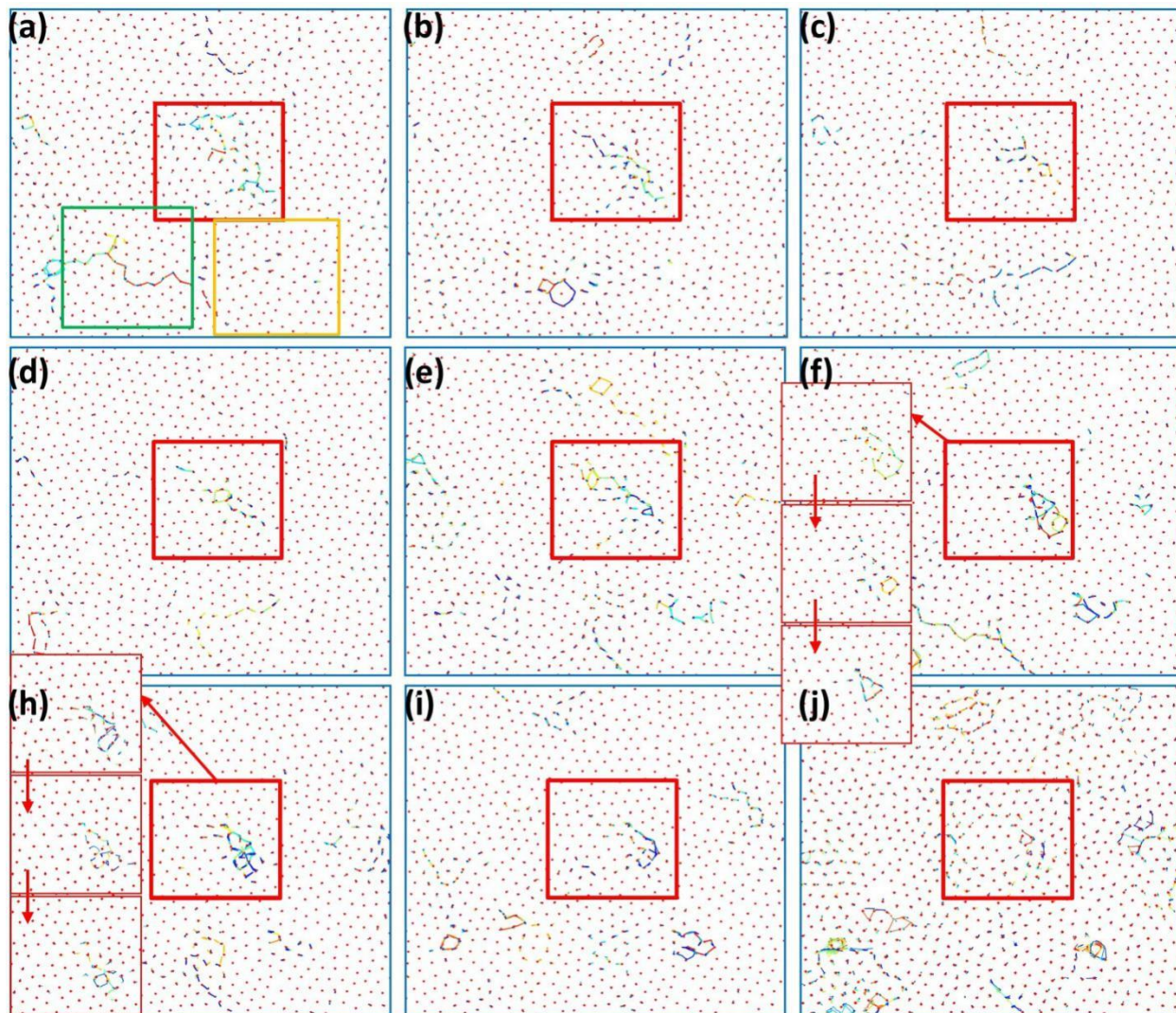


**Figure S21. Experimental Results:** (a) Coarse-grained trajectories from Figure S18 (c). (b)-(j) Consecutive time sequence of coarse-grained trajectories showing details of the dynamics in (a). Further details are shown in the insets in (f) and (h).



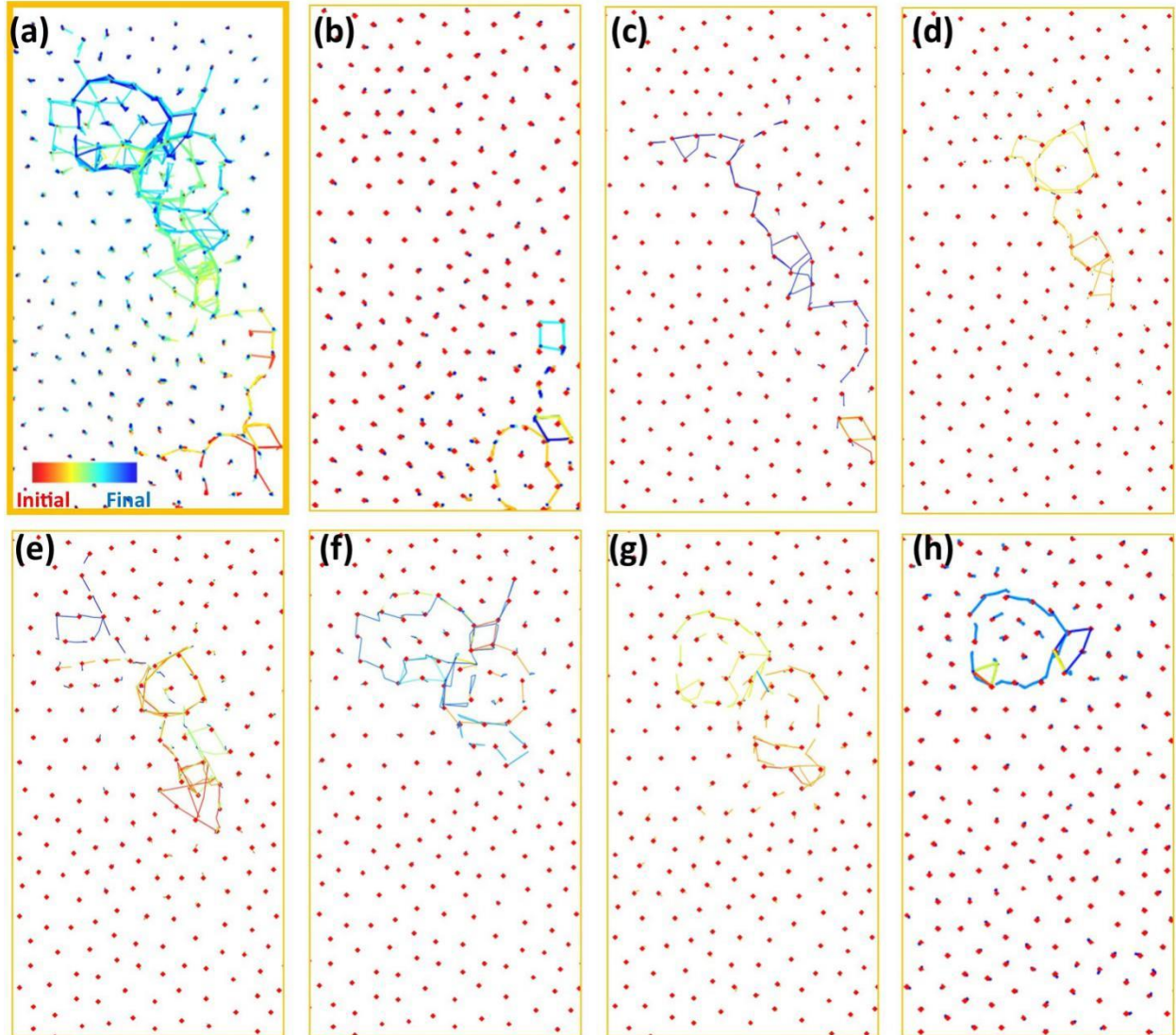


**Figure S22. Simulation Results of packing fraction  $\phi_{\text{MD}} = 0.810$ :** (a) Coarse-grained trajectories in a region with a core-like mobile cluster. (b)-(h) Consecutive time sequence of coarse-grained trajectories showing details of the dynamics in (a).

### 3. Supplementary Results on Glass-Crystal Coexisting Systems

We use unimodal colloidal systems to produce coexisting glassy and crystalline regions for demonstrating the reversible transformation between vacancies and quasi-voids. Once a sample is prepared, it exhibits a fully amorphous state. Then, crystalline regions emerge. After about 8 hours, we observe relatively stable coexisting glassy and crystalline regions. The phase boundaries show no significant evolution during hours of further observations.

We then study particle dynamics in these stabilized glass-crystal coexisting systems as already shown in Figure 2 in the main text. As an additional example, particle trajectories from a similarly prepared sample are shown in Figure S23. In both Figures 2 and S23, we visually identify the glassy and the crystalline regions subjectively. The precise locations of the boundaries may vary slightly if more precise phase identification criteria are used. However, the

existence of both highly ordered and highly disordered regions are evident visually not only from particle arrangements but also from the geometries of the particle trajectories.

From Figure S23(b), trajectories of neighbouring hopping particles join together to form a long string, in a generalized sense, extending from position 1 in the crystalline region to position 2 in the glassy region. The part of the string in the crystalline region takes the geometry of a random walk and is evidently caused by a vacancy. In the glassy region, it is instead generated by the motion of a quasi-void, which is induced by the vacancy as explained in the main text. The quasi-void then moves further to position 3, generating another string-like motion. It is evident that the free volumes of the quasi-void (fragmented blue areas) originate from the vacancy and should be comparable in areas.

We have observed dozens of similar examples of trajectories extending across glassy and crystalline regions in either direction. The alignments of the trajectories are excellent in almost all cases, even across the phase boundary. This is easily explained by introducing quasi-particles referred to as quasi-voids, which can reversibly transform into vacancies. However, such alignments cannot be explained by unorganized generic free volumes supplied by the vacancies. We have observed very long strings at large  $\phi$  in the glassy regions generated by the motions of individual quasi-voids. This shows that quasi-voids have long observable lifetimes. This qualifies it as a meaningful quasi-particle for describing glassy dynamics.

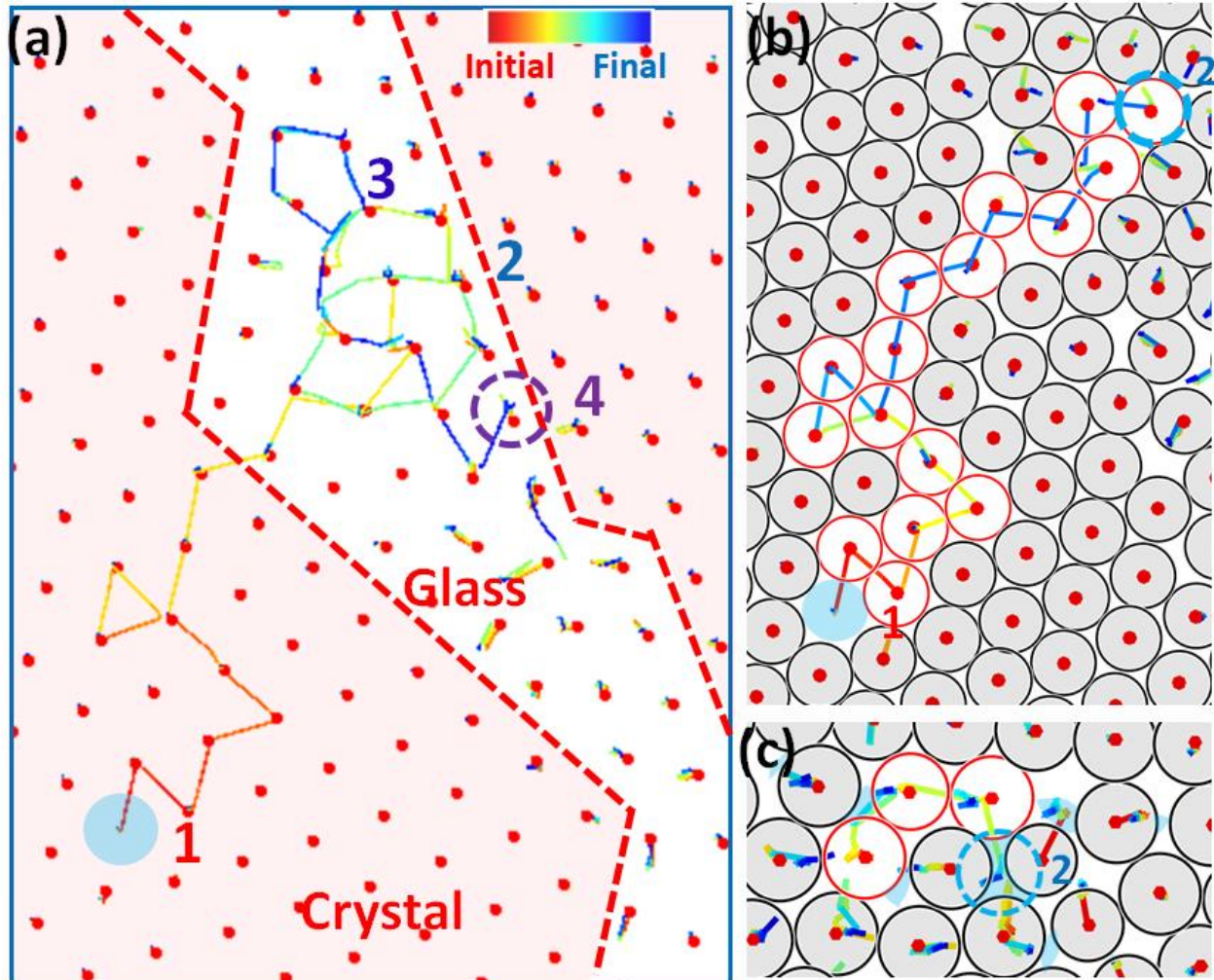


**Figure S23. Experimental Results:** (a) Coarse-grained particle trajectories in a coexisting glassy (white) and crystalline (red) system. A vacancy at position 1 induces a quasi-void at position 2 which further moves to position 3. (b) and (c) Particles and their trajectories showing two consecutive time subintervals of (a). Particles are shown at their initial positions of the subinterval. We observe the conversion of a vacancy (blue circle) into a quasi-void in (b). The resulting quasi-void consisting of fragmented free volumes (blue areas) and a further string-like motion it induces are shown in (c).

### References and Notes:

31. J. C. Crocker and E. R. Weeks, Particle tracking using IDL (<http://www.physics.emory.edu/faculty/weeks/idl/tracking.html>).
32. E. P. Bernard, W. Krauth, D. B. Wilson, Event-chain Monte Carlo algorithms for hard-sphere systems, *Phys. Rev. E* **80**, 056704 (2009).
33. M. Isobe, Simple and efficient algorithm for large scale molecular dynamics simulation in hard disk system. *Int. J. Mod. Phys. C* **10**, 1281-1293 (1999).

34. W. G. Hoover, E. Nathan, K. Hanson, [Exact hard-disk free volumes](#). *J. Chem. Phys* **70**, 1837-1844(1979).